NASA CR- 100700

THERMAL ABSORPTION IN SEEDED GASES

by
J. S. Cory and A. Bennett

Cover
on green stock

Prepared under Contract No. NASw-1697 by
McDonnell Douglas Astronautics Company - Western Division
Donald W. Douglas Laboratories
Richland, Washington
for
NATIONAL AERONAUTICS AND SPACE ADMINISTRATION

TITLE

THERMAL ABSORPTION IN SEEDED GASES

by

J. S. Cory and A. Bennett

Title Page
on grey stock

Prepared under Contract No. NASw-1697 by

McDonnell Douglas Astronautics Company - Western Division
Donald W. Douglas Laboratories
Richland, Washington
for

NATIONAL AERONAUTICS AND SPACE ADMINISTRATION

CONTENTS

SUMMARY

This document is the final technical report submitted under Contract No. NASw-1697 on February 7, 1969, and covers work from February 13, 1968 through February 12, 1969. This report is cataloged by McDonnell Douglas Astronautics Company--Western Division and the Donald W. Douglas Laboratories as Report No. DAC-60779. To study the concept of radiantly heated seeded aerosolsito temperatures at which the propellant for a gas-core nuclear reactor would become opaque, was made using hydrogen and helium gases seeded with micron-size particles and exposed to radiant energy from a high-power (40 kilowatts/cm^2) xenon flash tube.

The experimental apparatus consisted of an elliptical reflector which had as its foci the xenon flashlamp and a 6 by 1/2 inch quartz cylinder containing the aerosol. Temperature was determined by measuring the pressure in the constant volume quartz cylinder. Tantalum-carbide particles produced the highest temperatures, 5300° and 6600°K for hydrogen and helium respectively.

The theoretical model consists of spheres of gas with solid particles at their centers. The model includes reradiation from the particles, heat losses from the gas to the container, temperature dependent values for the heat capacities (seed and gas), and thermal conductivity (seed and gas). Qualitative agreement between this model and the experiment was good, but quantitatively, the theoretical temperatures were too high. Two phenomena were identified as the cause for the disagreement. These were evaporation of the particles, and the chemical reduction of the quartz cylinder inner

surface to silicon. Both phenomena reduce the incident energy on the particles, thereby reducing the temperature of the gas. Two reasonable analytical functions were assumed and included in the model with the result that the theory and experiment agree quantitatively.

Nothing was found during this program to indicate that the temperatures obtained in these flash heating experiments could not be obtained in a nuclear propulsion system radiantly transferring energy to a seeded gas.

INTRODUCTION

Improvements in the performance of a propulsion system are, to a large degree, achieved by increases in the exhaust velocity or specific impulse. In a conventional chemical rocket engine, exhaust velocity is limited by the temperature attainable by chemical reaction and the molecular weight of the resulting reaction products. Use of nuclear energy not only offers the potential of much higher temperature, but also allows an independent choice of low-molecular-weight propellants, both of which increase the specific impulse. One current nuclear-propulsion concept uses a fissioning gas (or gaseous fuel) separated from a seeded hydrogen propellant. This report documents a program by the Donald W. Douglas Laboratories to evaluate the characteristics of radiantly heated suspensions of solid particles in hydrogen.

Heat transfer between fissioning gaseous fuel and a hydrogen propellant is one of the major problem areas in a gas core nuclear propulsion system (ref. 1). In current concepts, the fissioning fuel and propellant remain separated, and energy must be transferred by thermal radiation at wave lengths in the visible and ultraviolet spectrums. At temperatures below 6000°K, however, equilibrium hydrogen is transparent to radiation at these wave lengths (ref. 2). Seeding the entering hydrogen with small absorbing particles appears to offer a solution to this problem. The particles are expected to absorb the thermal radiation and transfer this energy to the hydrogen by conduction, thus heating the hydrogen to temperatures where the hydrogen itself becomes opaque.

Since 1961, several groups have investigated radiant heat transfer to an aerosol to evaluate this concept. Lanzo and Ragsdale (ref. 3)

experimentally investigated the steady-state absorption of suspended particles as a function of material, size, and concentration; and investigated (ref. 1) heat transfer from an arc to a flowing aerosol. Masser (ref. 4) made an analytical study of radiant heating of an aerosol in a cavity reactor, assuming constant absorption and negligible reradiation from the aerosol. McAlister et. al. (ref. 5) reported on theoretical and experimental steady-state heat transfer from a hot cylindrical wall to a flowing aerosol. These results were in agreement with theory, but both experiments and theory were limited to a thermal radiation flux of less than 1 kw/cm^2 and aerosol temperatures of less than 2000°K. In the gas core reactor, in contrast, the flux is expected to be 40 kw/cm^2, with aerosol temperatures above 6000°K.

In a previous study at McDonnell Douglas (refs. 6 and 7), techniques were developed to extend these results to higher temperatures and thermal fluxes, both experimentally and theoretically. The experimental technique used a xenon flash tube and elliptical reflector to achieve 40 kw/cm^2 flux on the aerosol at the sacrifice of steady-state conditions. Temperature was measured in a constant volume gas thermometer containing the aerosol. Temperatures of 3700° and 6000°K were achieved in hydrogen and helium respectively. The theoretical development included thermal reradiation from the aerosol at high temperatures by writing an energy-balance equation around each particle and a unit cell of gas associated with that particle. This led to a non-linear description of a two-temperature radiation-heated aerosol. While the temperature profiles of the analytical model produced qualitative agreement with experimental observations, the quantitative difference was significant. These differences are related to the observation that the energy absorptivity of the aerosol decreased more rapidly with increasing time and temperature than is predicted by the model. No satisfying explanation was found for this phenomenon.

With this background, the present investigation was undertaken, utilizing this flash-heating technique expanded to handle higher energies, to answer two questions.

(1) What is the highest temperature obtainable with available flash-heating apparatus, and is this high enough to cause ionization?

(2) What is the reason for the decrease in energy absorptivity during the flash as observed in the previous study.

Most of the initial effort was concentrated on obtaining an experimental answer to the first question. The flash heating technique was extended to increase the specific energy available to the gas from 250 to 7000 joules per mg of hydrogen by:

(1) Increasing the flash tube output

(2) Transferring more of the flash energy to the test volume

(3) Increasing the optical density of the test aerosols

(4) Reducing the density of the gas in the test cell

This energy-density increase did not produce a corresponding temperature increase because of the increased radiation losses at high temperatures. With this energy increase, however, hydrogen and helium temperatures of 5300° and 6600°K respectively were observed. The hydrogen temperature is sufficiently high to produce some ionization and plasma absorption, even in equilibrium hydrogen. Ionization was observed in helium by measuring the conductance of the aerosol during the flash. Thus, an affirmative answer is given to the second part of Question 1.

The second question was answered only after aerosol interactions with the quartz test cell and radiant heat transfer to the aerosol were considered. The observed decrease in the fraction of available thermal radiation energy absorbed by the aerosol was found to be the result of increased absorption at the quartz wall, as well as decreased absorption by the aerosol resulting from evaporation of the particles. The superheated aerosol particles evaporate, thereby reducing aerosol absorption. Of more importance in the flash-heating experiments, this particle vapor condenses and reacts chemically with the quartz, thereby reducing the energy reaching the aerosol and, consequently, reducing the overall rate of radiant heat transfer from

the flash-tube to the aerosol. The anomalous absorptivity observed in the flash-heating experiments is important, therefore, in propulsion system concepts based on a transparent partition.

The sections which follow present the information used to answer the two questions. In the next section, the theoretical background is presented. Four phenomena, quartz wall sorption, aerosol effective emittance, plasma production and energy absorption, and radiant heat transfer to the aerosol are important in explaining the experimental results. Theories were available for the first three of these phenomena. Since considerable development was required to adequately describe the fourth, it is presented in more detail. Following the theoretical presentation, experimental procedures and data reduction techniques are discussed. Finally, experimental results and the reasoning used to explain the observed energy absorptivity are presented, followed by the conclusions which were drawn.

THEORY

Each of the four phenomena, quartz wall sorption, aerosol effective emittance, plasma production, radiant heat transfer, which dominate the observed experimental behavior has been studied under other conditions. Langmuir and his successors investigated adsorption and chemisorption on surfaces at cryogenic and room temperatures in high vacuums. Electromagnetic theory provides a firm understanding of energy absorption by monodispersions of small particles. Inverse bremsstrahlung energy absorption by plasmas and plasma generation by thermionic emission from particles in an aerosol are well established phenomena at temperatures respectively higher and lower than temperatures encountered in the present experiments. Similarly, radiant heat transfer through a participating medium has been thoroughly studied, but only at low temperatures.

With the exception of heat transfer in an aerosol, it is beyond the scope of this study to attempt to extend these theories to high density polydispersions at 5000°K. The complexity of the calculations required makes this extension a formidable task, and the experimental data required to quantitatively confirm the theories was not obtained. As these stand, however, the theories of wall sorption, particle-energy absorption, plasma creation, and plasma energy absorption are sufficiently well developed to offer considerable insight into the phenomena observed in the present experiments. A brief summary of each follows.

Quartz Wall Sorption

In the flash-heated aerosol, even particles of refractory materials are heated above their boiling point. Evaporation of this material (refs. 8 and 9) creates a hot gas, bounded by relatively cold quartz walls. Vapor molecules diffuse to and strike the walls at high velocity.

According to Langmuir (ref. 10), when gas molecules impinge against a solid, they do not rebound elastically but condense on the surface, being held by the field of force of the surface atoms. These molecules may subsequently evaporate from the surface. The time that elapses between the molecular condensation and subsequent evaporation depends on the intensity of the surface forces and the temperatures of the surface. Adsorption is the direct result of this time lag. If the surface forces are relatively intense, as when a chemical reaction occurs between the gas and the surface, evaporation occurs at a negligible rate, so that the surface becomes completely covered.

The most widely used quantization of this hypothesis was derived by Brunaur, Emmett, and Teller as:

$$\frac{P}{V(Po-P)} = \frac{1}{V_m C} + \frac{(C-1)}{V_m C}\frac{P}{Po}, \qquad (1)$$

where P is the partial pressure of the sorbed gas, Po its saturation pressure, and V is the volume of gas adsorbed. V_m and C are both temperature-dependent measures of the number of condensation or reaction sites and the flux of vapor molecules to the surface. Figures 1 and 2 (ref. 10) show the isobars and five types of isotherms (observed experimentally) which are predicted by this equation.

This relation has been repeatedly verified (ref. 10). Experiments, correlated by this equation, have separately demonstrated all of the surface phenomena observed in the flash-heating experiments: multilayer condensation, chemisorption at higher temperatures with subsequent condensation at lower temperatures, and desorption by increasing the temperature of the surface. To use this relation to predict quartz wall sorption in the flash-heating experiments, however, would require determination of the values and the temperature dependence of V_m and C at the temperatures of interest for each particle material. These data are not available, and the theory of wall sorption can be used only qualitatively in connection with the flash-heating experiments. As shown in the discussion of experimental results, however, the type of behavior predicted by Equation 1 is consistent with the flash-heating results.

Aerosol Emittance

The ability of a cloud of particles to absorb or emit electromagnetic radiation has been extensively studied (ref. 11). For monodispersed (single size) spheres, an exact theory is available for calculating the absorbance and emittance from the particle absorption cross-section, $Q^{(a)}$, extinction

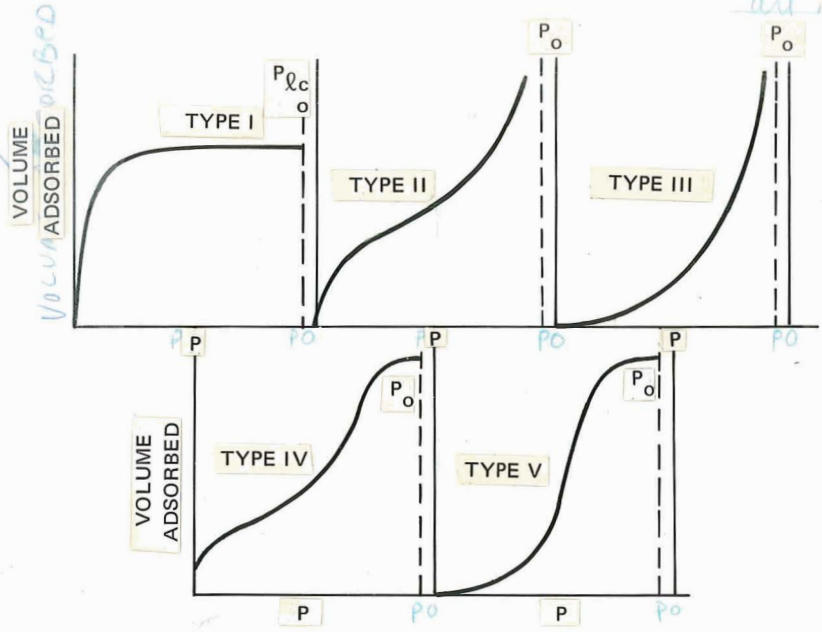

Figure 1. Five Isotherm Types Predicted by Equation 1

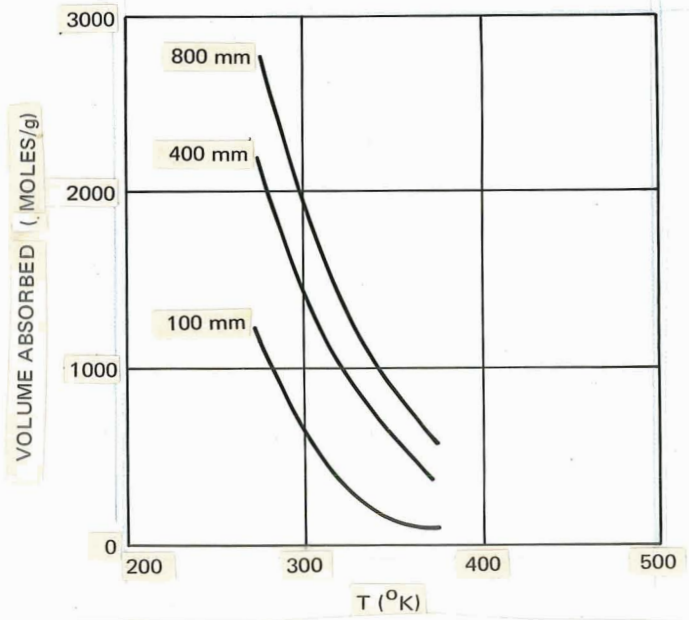

Figure 2. Isobars Correlated by Equation 1

cross section, $Q^{(e)}$, number density, N, thickness, x, and incident or emitted wave length. For polydispersions of non-spherical particles, the basic theory is valid, but exact calculations are impractical because of the required integration over the source wavelength distribution. When the dependence of Q on the wavelength of the incident light is not important, the radiation properties of a non-spherical polydispersion may be adequately described (ref. 12) by assuming a superposition of monodispersed spherical particles. This is the procedure used in the discussion which follows. Consider a beam of light with cross-section A_L passing through an aerosol. The reduction in A_L ($-dA_L$) in distance dx is equal to the cross-section of particles in the volume A_L dx, because these particles absorb or scatter from the beam the light they intercept as

$$-dA_L = (\Sigma_i Q_i^{(e)} {}_i N_i) A_L dx \tag{2}$$

where $Q^{(e)}$ = particle cross section, $Q_i^{(e)}$ = cross section of the $i^{\underline{th}}$ particle size with number density per unit volume of N_i, and the sum is over all particle sizes. For spherical particles, $Q_i^{(e)} = B\pi a_i^2 = BAp_i/4$, where Ap_i is the total surface area of the $i^{\underline{th}}$ particle. Then, if B is the same for all particle sizes,

$$\Sigma Q_i^{(e)} N_i = \Sigma \frac{B}{4} Ap_i N_i = \frac{BAp}{4Vg}, \tag{3}$$

where Ap is the total surface area of all the particles in volume Vg. Solving Equations 2 and 3,

$$\frac{A_L}{A_{Lo}} = \exp\left(-\frac{BAp}{4Vg} x\right), \tag{4}$$

where it was assumed the particle cross-sectional area/volume (BAp/4Vg) was constant over distance x. In the flash-heating experiments, the distance x is the cylinder diameter, which can be written in terms of the cylinder surface area, Aw, and volume, Vg, as

$$x = \frac{4Vg}{Aw} = 4\frac{\pi x^2 L/4}{\pi x L} \tag{5}$$

which allows Equation 4 to be written as

$$\frac{A_L}{A_{Lo}} = \exp\left(-\frac{BAp}{A_W}\right). \tag{6}$$

Coefficient B is not necessarily the same for all very small dielectric particles because of resonance effects. For dielectric particles with a radius, a, very much smaller than the wavelength of interest, λ, coefficient B varies as the fourth power of $2\pi a/\lambda \sim 1$ to produce the resonance phenomena of Mie scattering (ref. 11). However, only a small imaginary component to the index of refraction is required to damp these resonances, as shown in Figure 3 (ref. 11). The radius of the particles used in the experiments are at least one tenth of the wavelengths of interest (usually $a \simeq 2\lambda$) and have appreciable electrical conductivity, so the assumption that coefficient B is independent of size is reasonable.

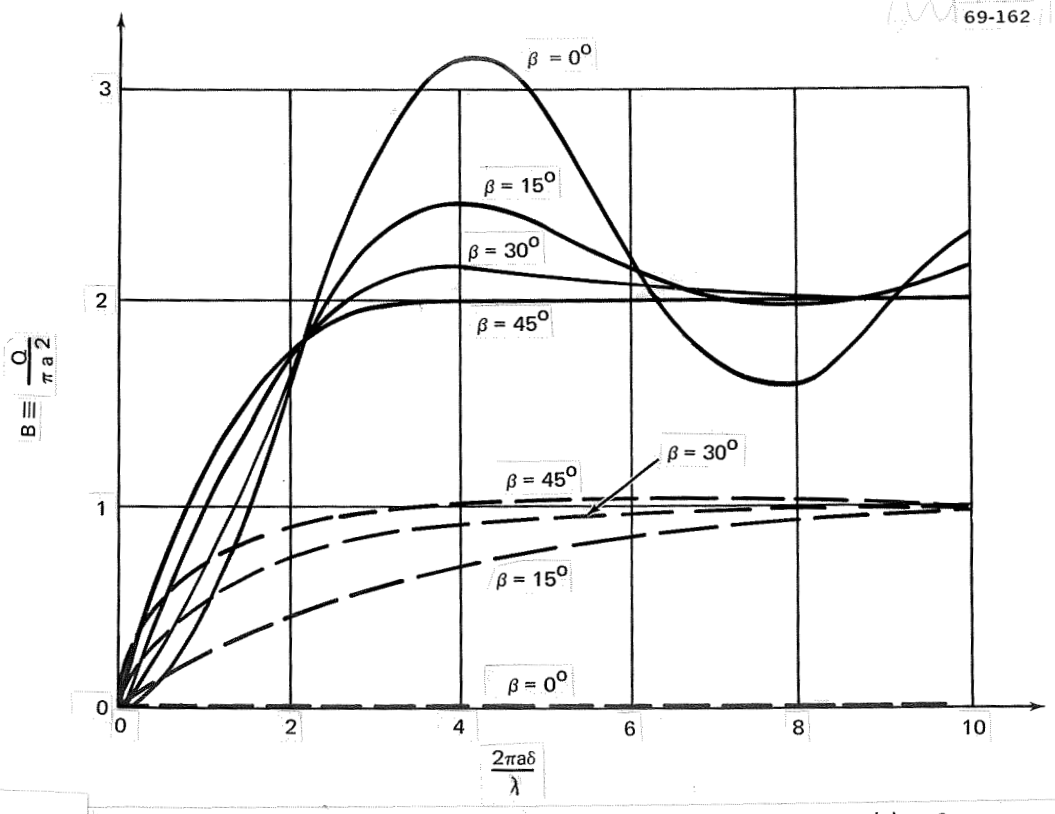

Figure 3. The Extinction Curves $Q/\pi a^2$ (Full Lines) and the Absorption Curves $Q^{(a)}/\pi a^2$ (Interrupted Lines) for Weakly Absorbing Spheres of Refractive Index $\hat{\eta} = (1 + \delta) + i\delta \operatorname{Tan} \beta$ where δ is Real and Small Compared to Unity.

As shown in Figure 3, the value of coefficient B to be used in Equation 6 depends on the quantity to be measured. Coefficient $B = 2\,(Q^{(e)}/\pi a^2)$ should be used in transmittance measurements; $B = 1\,(Q^{(a)}/\pi a^2)$ is the correct value for calculating the energy absorbed by the particles. The optical transmittance, α, and the fraction, F_D, of energy absorbed from a beam of light are related, therefore, by

$$\ln\alpha = 2 \ln (1-F_D). \tag{7}$$

In the flash heating experiments, all of the rays of light from the flash tube do not traverse a full diameter. Some travel a much shorter distance, through a chord of the cylindrical test chamber; others have a component along the cylinder axis and traverse a longer distance. The net effect of this process has been calculated (ref. 5) by assuming an isotropic source and, for the cylinders used in the experiment (L/D = 13), is adequately described by Equation 6 with a multiplicative correction as

$$F = 0.9294F_D = 0.9294 \quad [1 - \exp(-Ap/A_W)]. \tag{8}$$

The fraction F, defined by Equation 8 can also be considered as the aerosol-wall view factor. The view factor between two surfaces, $F_{1,2}$, is defined as the fraction of radiation leaving surface A_1 (in all directions) which is intercepted by surface A_2 (ref. 13). The factor, F, is therefore the view factor between the total particle surface area, $A_2 \equiv Ap$, and the surface area of the test chamber wall, $A_1 \equiv A_w$. A simple derivation based on the second law of thermodynamics (ref. 13) shows that these terms may be used to define G, the fraction of the energy radiated by the particles which reaches the wall as

$$G A_p = F A_w. \tag{9}$$

The remainder, 1-G, is then the radiant energy interchange between the particles. The factor G is also the effective emittance of the aerosol and can be related to the measured transmittance or to the particle total surface area by combining Equations 6 through 9 as

$$G = 0.9294 \frac{A_W}{A_P} \left[1 - \exp\left(-A_P/A_W\right)\right] \tag{10A}$$

or

$$G = \frac{-1.8588}{\ln \alpha}\left(1-\alpha^{1/2}\right). \tag{10B}$$

Plasma Production and Energy Absorption

At the temperatures of the flash-heating experiments, each particle thermionically emits electrons. Because the particles are electrically isolated, however, each emitted electron leaves behind a positive charge on the particle. This positive charge creates a potential well around the particle, possibly trapping the electron into a closed orbit. As subsequent electrons are emitted, the potential well deepens until an equilibrium is reached where the rate of thermionic emission is equalled by the rate-of-arrival of electrons trapped into closed orbits.

This equilibrium condition is described by Equations 11, 12, and 13 (ref. 14) as

$$V(r) = (Z_p e/4\pi\epsilon a) - (Z_p e - 4\pi e\int_a^r n_e r^2 dr)/4\pi\epsilon r, \tag{11}$$

where V is the potential and r is measured from the center of the spherical particle of radius a, Z_p is the charge on the solid particle, e is the electronic charge, ϵ is the emissivity, and n is the electron density around the particle. Assuming Maxwellian velocity distribution of these electrons, their density is given by

$$n_e(r) = n_{ea}\exp(-eV/kT), \tag{12}$$

where k is the Boltzmann constant, T is the temperature of the particles, and n_{ea} is the density of electrons at radius a, which is given by equating the thermionic current density to the current density of electrons in a cavity as

$$n_{ea} = n_{es} \exp [-\phi/kT], \tag{13}$$

where ϕ is the thermionic potential energy and n_{es} is the density of conduction electrons in the solid phase. For a metal at high temperatures, $n_{es} \simeq$ (total electron concentration in the solid) X $\exp(-\varepsilon_F/kT)$, where ε_F is the energy of the Fermi level. For an insulator, the number of free electrons are fewer and their distribution is Maxwellian.

A typical solution to these equations is shown in Figure 4, (ref. 14) for a one-micron zirconia particle at 3000°K in a bounded volume of radius 10 microns, $Z_p = 206$, $Z_p e^2/4\pi\varepsilon akT = 2.27$, $n_{ea} = 4.62 \times 10^{18}/m^3$, and argon density of $10^{20}/m^3$.

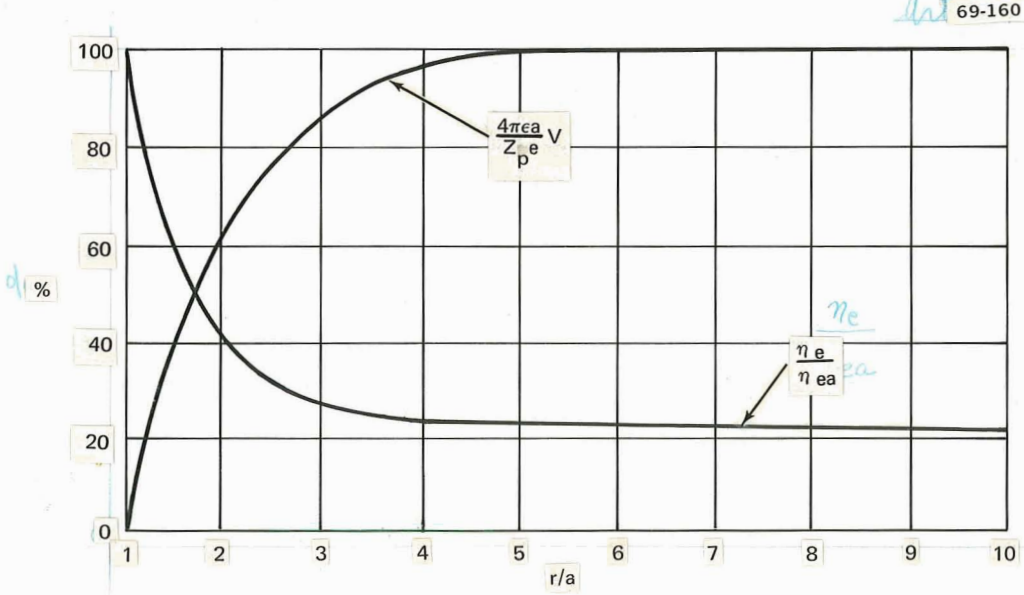

Figure 4. Distribution around a Solid Particle in 3000°K Argon

The system appears as a large multiply (206 times) charged nucleus surrounded by a cloud of orbiting electrons. These electrons, by momentum exchange with the electric field, can capture and emit photons by inverse bremsstrahlung (refs. 15 and 16).

The ionized particle system is similar to a fully ionized plasma (ref. 16) and the photon absorption coefficient is given by (ref. 15)

$$k_\nu = \frac{4}{3}\left(\frac{2\pi}{3kT}\right)^{1/2} \frac{n_e n_i Z_p^2 e^6}{hcm_e^{3/2}\nu^3} \text{ cm}^{-1}. \tag{14}$$

With a particle number density $n_i \simeq 10^9$/cc, a collision frequency $\nu = 5\text{x}10^{10}$/sec, and a temperature of 3000°K, the ratio of the plasma absorption coefficient, $K_{\nu p}$, to the geometric absorption coefficient, $K_{\nu g}$, is

$$\frac{K_{\nu p}}{K_{\nu g}} = 1.7 \text{ x } 10^{-9} Z_p^3. \tag{15}$$

Because the thermionic emission from a particle depends exponentially on the temperature, and $Z_p \sim 200$ at only 3000°K, it is reasonable to expect plasma absorption to be significant compared to geometric absorption at the particle temperatures of the flash-heating experiments.

Radiant Heat Transfer to an Aerosol

The following theory of radiant heat transfer to an aerosol was derived to emphasize the role of reradiation by the particles. Attention is focused on determining the time-dependent temperature of the particles to specify the total energy radiated by the particles. The optically thin approximation is unsuitable for this approach, despite the considerable simplification which would result. A compromise was selected whereby the temperatures

and radiation fluxes were assumed uniform throughout the volume, but these uniform fluxes were modified by the real optical thickness of the aerosol.

The result of this approach is a two-temperature model of an aerosol incorporating the mechanisms illustrated in Figure 5. The particles and gas are not in equilibrium. The elevated particle temperature accentuates the radiation loss from the aerosol and shows that previous treatments of this problem, which neglect (refs. 4 and 17) or add reradiation as an afterthought, seriously overestimate the net radiation absorptivity of an aerosol. Especially at the high energy flux (~40 kw/cm^2) in a gas core reactor, particle superheating must be considered.

The basis for this derivation are energy balances written around each particle and around the entire volume of gas incorporating the mechanisms illustrated in Figure 5. For a given particle

$$P_s + P_r + P_g = P_a, \tag{16}$$

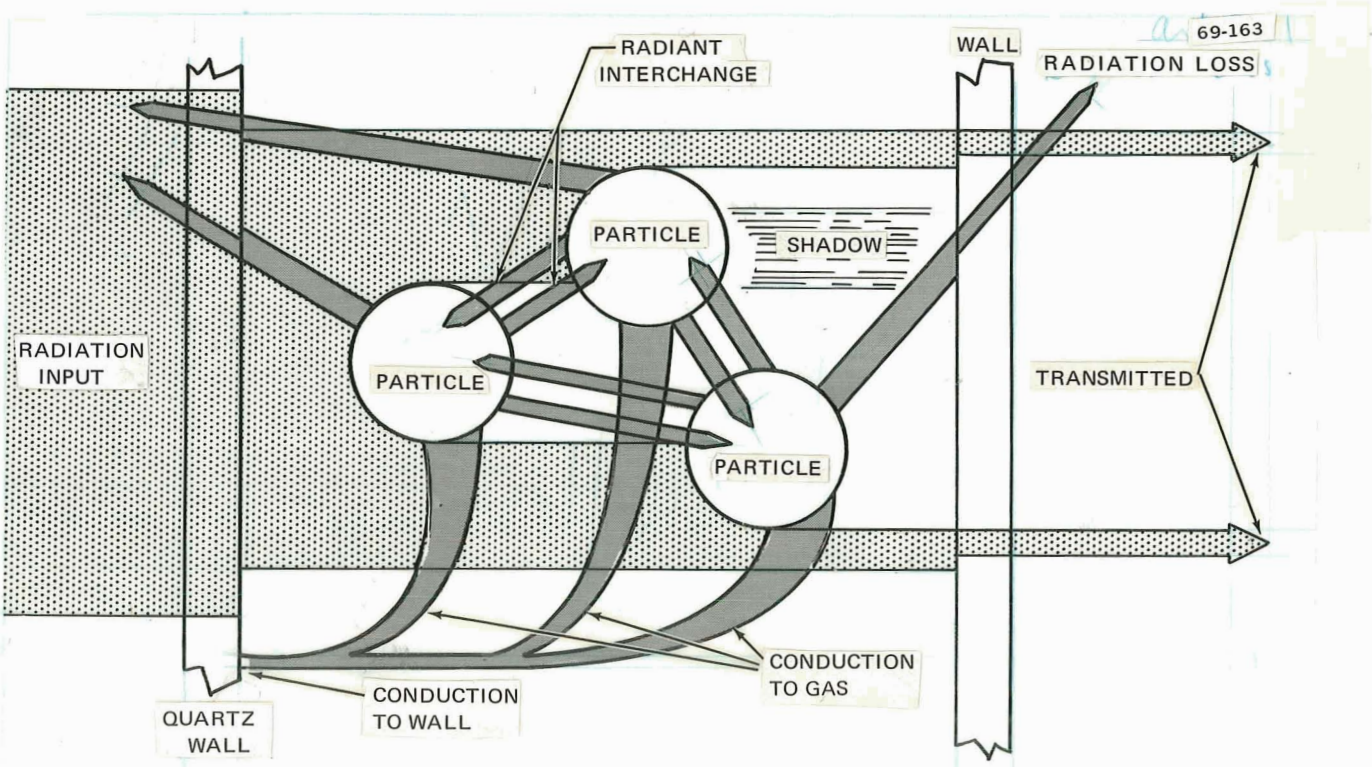

Figure 5. Heat Transfer Mechanisms in an Aerosol

where the subscripts s, r, g, and a refer respectively to the rate of energy stored, radiated, conducted to the gas, and absorbed from the radiation field. For the gas

$$P_{sg} + P_w = \Sigma P_g, \tag{17}$$

where the subscripts sg and w refer respectively to the rate of energy storage in the gas and conduction to the wall, the sum over P_g is the rate of energy conduction to the gas by all of the particles.

Four of the six terms in Equations 16 and 17 are easily defined. The rate of energy storage in each particle and the gas is given by

$$P_s \equiv \frac{4}{3} \pi a^3 \rho c \frac{dT}{dt} \tag{18A}$$

and

$$P_{sg} \equiv V_g \rho_g c_g \frac{dT_g}{dt}, \tag{18B}$$

where a is the particle radius, ρ and c the density and mass specific heat capacity of the particle, T and T_g respectively the particle and gas temperatures, and V_g, ρ_g, and c_g the gas volume, density, and mass specific heat capacity at constant volume. Implicit in these definitions is the assumption that the entire gas volume is at a single temperature. The rate of energy loss by the gas to the wall and by a particle to the radiation field is given by

$$P_w \equiv HA_w (T_g - T_w) \tag{19}$$

and

$$P_r \equiv 4 \pi a^2 \varepsilon \sigma T^4, \tag{20}$$

where A_w and T_w are the wall area and temperature, H is an effective (conduction plus convection) heat transfer coefficient, ε is the particle emittance, and σ the Stefan-Boltzmann constant. Each of the material properties used in these definitions may be functions of time or temperature, and the only assumptions so far are that both materials may be satisfactorily described by a single-state variable.

Additional approximations are used in defining the rate at which energy is absorbed from the radiation field and conducted to the gas. In the case of P_a, these approximations are concerned with defining the radiation flux. The rate at which radiant energy is incident on all of the particles may be written as

$$\Sigma P_a \equiv \Sigma 4\pi a_i^2 \varepsilon \phi_i, \tag{21}$$

where the sum is over all particles and ϕ_i is the (isotropic) flux on the $i^{\underline{th}}$ particle. In accordance with the semi-optically thin assumption mentioned above, it is assumed the ϕ_i are identical for all particles. Then Equation 21 may be rewritten as

$$\Sigma P_a = \varepsilon \phi A_p, \tag{22}$$

where A_p is the total particle area and ε is the particle absorbance (assumed equal to the emittance).

The flux, ϕ, incident on each of the particles has two components: flux from the outside, ϕ_1, and flux from all of the other radiating particles, ϕ_2. Flux ϕ_1 is specified by the form factor F as

$$\varepsilon A_p \phi_1 = (\Sigma P_a)_1 = \varepsilon \phi_w A_w F, \tag{23}$$

where ϕ_w and A_w are the wall flux and area. Flux ϕ_2 is related to form factor G by

$$\varepsilon A_p \phi_2 = (\Sigma P_a)_2 = \varepsilon(1 - G)\Sigma 4\pi a^2 \varepsilon \sigma T^4, \tag{24}$$

where 1 - G is the fraction of the energy radiated by all of the other particles, $\Sigma 4\pi a^2 \varepsilon \sigma T^4$, which does not escape from the aerosol. Using the general aerosol relation between F and G from Equation 9, the rate of energy absorption by a given particle from the total radiation field may be written as

$$P_a \equiv 4\pi a^2 \varepsilon(\phi_1 + \phi_2) \tag{25A}$$

$$= \frac{4\pi a^2 \varepsilon}{Ap} \left[F A_w \phi_w + \left(1 - \frac{A_w}{A_p} F\right) \left(\Sigma 4\pi a^2 \varepsilon \sigma T^4\right) \right], \qquad (25B)$$

where the sum extends over all particles except the particle in question.

The rate of energy transfer from a particle to the gas may be found from the time-dependent conductive heat-transfer equation. The heat-transfer equation for central heating of a spherical volume of gas with adiabatic walls is

$$-K\frac{dTg}{dr} = \frac{c_g \rho_g \frac{4}{3}\pi (R^3 - r^3)}{4\pi r^2} \dot{\theta}, \qquad (26)$$

where K is the gas thermal conductivity, $\dot{\theta}$ the local rate of gas temperature change, and R the radius of the gas sphere. This equation, with $\dot{\theta}$ independent of position, is a reasonable description of the aerosol. Near the particle, the temperature gradient will be large and probably time dependent. At large distances from the particle, however, the finite amount of heat is conducted through a much larger area, and the temperature gradient associated with this conduction will be small. Further, only small changes in the absolute value of the gradient are possible. At the test cell walls, R is so large that it is reasonable to assume the wall to be adiabatic and that $\dot{\theta}$ is independent of position. With these assumptions, and, in the limit of large R Equation 26 may be integrated to yield,

$$\frac{4}{3}\pi R^3 \rho_g c_g \frac{dT_g}{dt} \simeq 4\pi a^2 \frac{K}{a} (T_a - T_g), \qquad (27)$$

where a is any specified inner radius. Equating the radius, a, to the particle radius and T_a to the particle temperature, it is apparent that Equation 27 gives the energy conducted to the gas for a single particle as

$$P_g = 4\pi a^2 \frac{K}{a} (T - T_g). \qquad (28)$$

Combining Equations 16 through 20, 25, and 28 gives the desired set of non-linear, coupled differential equations describing the time-dependent behavior of a radiantly heated aerosol as

$$\frac{4}{3}\pi a^3 \rho c \frac{dT}{dt} = 4\pi a^2 \left\{\varepsilon \left[FA_w \phi_w + (1 - G)\left(\sum_i 4\pi a_i^2 \varepsilon \sigma T_i^4\right) - \sigma T^4\right] - \frac{K}{a}(T - T_g)\right\} \quad (29)$$

$$V_g \rho_g c_g \frac{dT_g}{dt} = \sum_i 4\pi a_i^2 \frac{K}{a_i}(T_i - T_g) - HA_w (T_g - T_w) \quad (30)$$

For N particles, there are N differential equations of Type 29 and one of Type 30.

A computer program was written to integrate Equations 29 and 30 by an iteration technique. Provisions were made to include a range of particle sizes, step-wise temperature dependence of ε, c_g, c, and K to allow for the effects of evaporation and dissociation. The quantity F (and G) is calculated from the measured transmittance, α, according to Equations 7 through 10. An arbitrary time dependence of the thermal radiation flux at the wall, ϕ_w, is acceptable.

The computer program was used to investigate the predicted effect of material and aerosol properties on the gas and particle temperature history. This investigation was not exhaustive, but several significant conclusions were reached. First, with particles less than 0.1 micron in diameter, the particles are tightly coupled to the gas. Both have essentially the same temperature, even at 40 kw/cm^2 input flux, and the whole problem may be described more easily as an absorbent gas. Suspensions of particles this finely divided is extremely difficult to obtain, however, so this behavior is not common. In the flash-heating experiments, agglomeration increased the particle radius from the fundamental crystal radii of about 0.1 micron to over 1 micron.

Superheating of the particles begins to be important in the size range of 0.1 to 1 micron in diameter. A typical computer plot of the solution to Equations 29 and 30 for 1-micron particles is given in Figure 6. Particle temperature is a few hundred degrees higher than the gas temperature, so radiation loss is up ~20% and the net energy absorptivity is also ~20% lower than would be calculated, assuming equal gas and particle temperatures. Within this size range, higher gas heat conductivity or lower gas heat capacity will bring the two temperatures closer together. Particle emittance, particle heat capacity, and aerosol transmittance have little effect on the particle-gas temperature difference.

Radiation losses are dominated by the largest particles in a size distribution, and, if a measurable fraction of the particles are larger than one micron, the particles are much hotter than the gas. The precise temperature difference is strongly dependent on aerosol and material properties and the radiation flux. With typical aerosols, however, particle temperatures 20% greater than gas temperatures are common. In these cases, calculations based on radiation at the gas temperature would overestimate the net energy absorptivity by 100%. Most aerosols can be expected to contain an appreciable fraction of particles or agglomerates with diameters greater than one micron, and therefore, it will usually be necessary to use a two-temperature theory in radiant heat transfer calculations.

EXPERIMENTAL PROCEDURES

The unique feature of the flash-heating experimental technique is its ability to generate a high (~40 kw/cm^2) flux of thermal radiation. The major drawback of this technique is the short duration of the flash. The several-milliseconds flash is sufficiently long for all of the physical processes involved to reach steady state (refs. 9, 10, and 16) but measurement techniques, especially for gas temperature, are a problem. This problem was

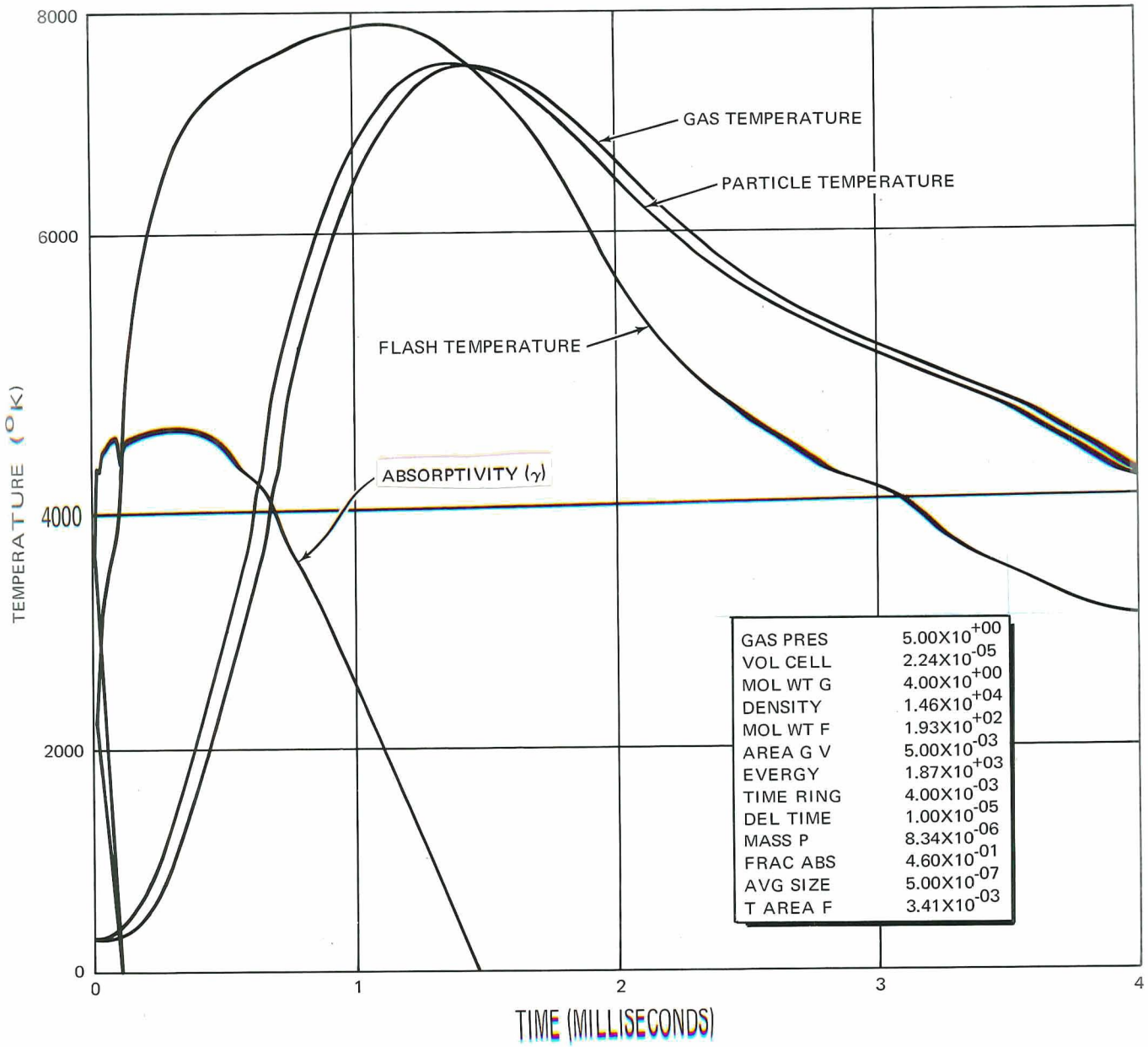
8000
6000
4000
2000
0
TEMPERATURE (°K)
0
1
2
3
4
TIME (MILLISECONDS)
GAS TEMPERATURE
PARTICLE TEMPERATURE
FLASH TEMPERATURE
ABSORPTIVITY (γ)
GAS PRES 5.00X10+00
VOL CELL 2.24X10-05
MOL WT G 4.00X10+00
DENSITY 1.46X10+04
MOL WT F 1.93X10+02
AREA G V 5.00X10-03
EVERGY 1.87X10+03
TIME RING 4.00X10-03
DEL TIME 1.00X10-05
MASS P 8.34X10-06
FRAC ABS 4.60X10-01
AVG SIZE 5.00X10-07
T AREA F 3.41X10-03

solved by enclosing the aerosol in a constant-volume test cell and measuring the gas-pressure history. This measurement can then be transformed to an average gas-temperature history when the number of moles of gas is known.

Figure 7 shows the apparatus which was constructed to utilize this technique in this program. Electrical energy, stored in capacitor banks, is discharged through inductors to a xenon flash tube. The light from the flash tube is focused by an elliptical reflector on a 6 by 1/2 in. test chamber. During the period starting two hundred milliseconds before the flash, this test chamber is filled with an aerosol by venting hydrogen or helium through a particle-dispersion apparatus, through a check valve, and into the evacuated test cell. A more complete description of the apparatus is given in Appendix A.

The apparatus contains several improvements over the equipment used in the previous investigations under Contract No. NASw-1310. The electrical energy storage capacity has been doubled and, with the addition of the spark-gap triggers to prevent spontaneous firing of the flash tube, the energy which can be delivered to the flash tube has been increased from 8 820 to 49 000 joules. Four additional inductors are now available which, with the additional capacity, have increased the available flash duration from 2.2 to 12 milliseconds. Relatively less has been done with the particle-dispersion apparatus but, by cleaning the gas passages, the achievable optical opacity $(1-\alpha)$ was increased from ~0.50 to 0.95 at an initial pressure of 5 atmospheres. A surge tank was also added to the gas lines, allowing initial pressures of less than one atmosphere.

Three time-dependent parameters are independently measured for each flash test: pressure, transmittance, and flash power. The pressure history is measured with a piezoelectric pressure transducer mounted in the bottom of the test chamber. The transmittance is measured by passing a laser beam through a diameter of the test cell and focusing the beam on the slits of a spectrometer set at 6328 Å. The flash power history is measured by a photodiode viewing the flash lamp.

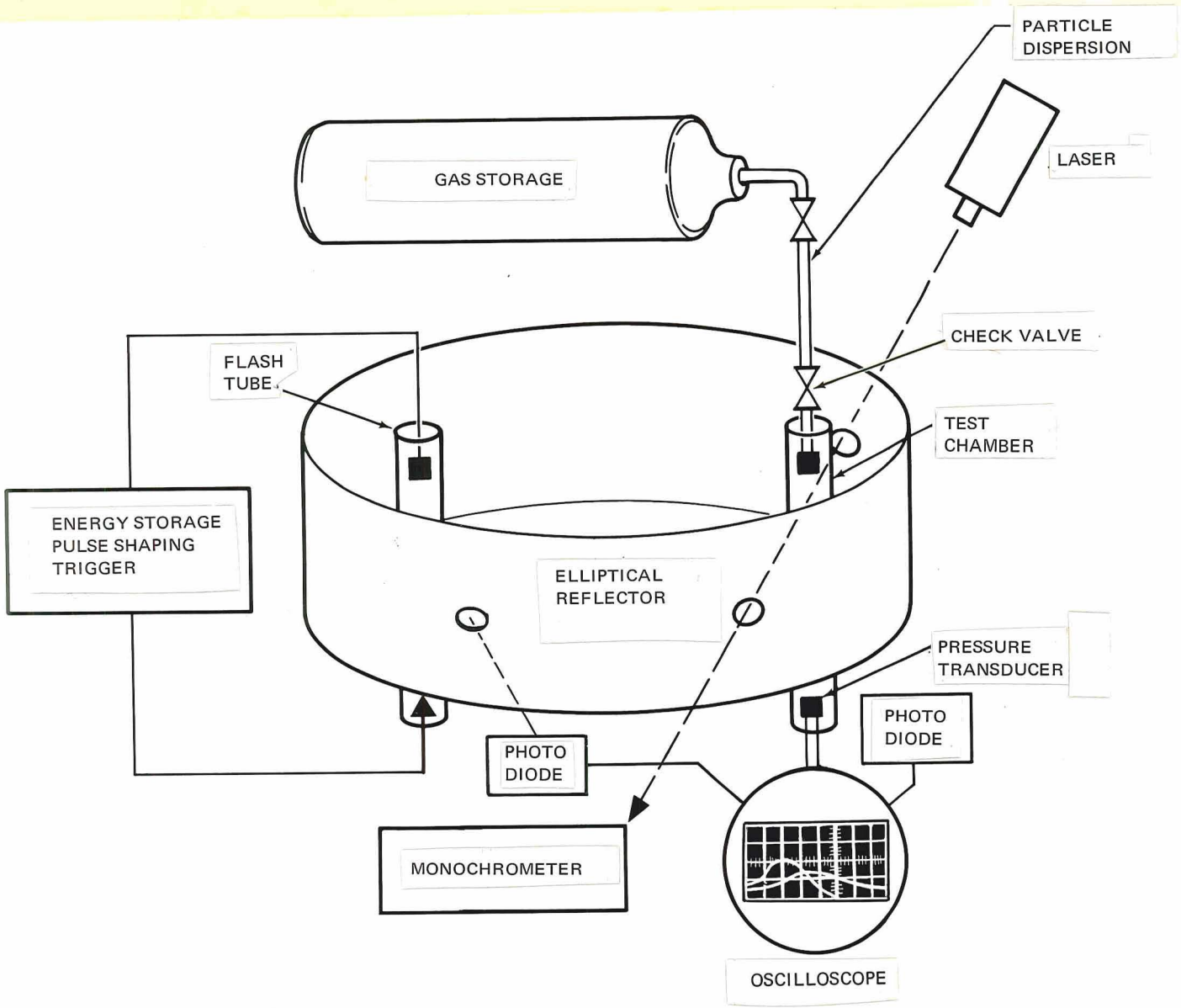

Figure 7. Experimental System

In addition, five parameters are frequently measured to characterize the aerosol and calibrate the time-resolved measurements. Initial pressure is measured both with the piezoelectric transducer and a thermocouple gauge. Total flash energy is measured with a carbon rod calorimeter inserted in the test cell. The mass of particles dispersed for a range of transmittances is determined by weighing a sealed test cell before and after loading the aerosol. Particle size distribution is determined by sampling the cold aerosol with a clean vertical surface in the test chamber, obtaining electron photomicrographs, and counting the image size distribution. Aerosol uniformity is checked by measuring transmittance at three axial locations. The procedures, equipment, and accuracy of these measurements are discussed in Appendix A.

A mechanized procedure was established to analyze the large amount of data obtained from over 500 flash tests. A line-follower feeding an analog-to-digital converter was used to digitize the pressure and flash-power history information from Polaroid photographs of the oscilloscope trace. A computer program used these data and real gas properties to compute the aerosol temperature and apparent absorptivity histories for all flash tests. Appendix B describes the procedures and capabilities of these data reduction proceedures in detail.

EXPERIMENTAL RESULTS

In this investigation, more than 2000 experiments were used to investigate the energy absorptivity properties of aerosols and to determine the highest temperature attainable with the flash-heating apparatus modified. Most experiments involved tantalum carbide particles dispersed in hydrogen or helium. Some data were also obtained for bromine gas, carbon dioxide gas, and aerosols containing carbon, iron, sulfer, tungsten,

aluminum, silica, talc, platinum, iron oxide, aluminum oxide, barium carbonate, and calcium carbonate.

The results presented in this section represent that portion of the experimental data directly pertinent to the main objectives of this investigation. First, a discussion of the role and timing of each of the four phenomena, discussed in the Theory section, is presented together with experimental results showing that these phenomena dominate the observed behavior. This phenomenological picture, which is consistent with experimental observations, explains the observed low energy absorptivity. A catalog of the maximum gas temperatures is then presented as functions of flash energy, flash duration, initial gas pressure, and aerosol transmittance. These data show that no absorption window exists in heating a tantalum-carbide-hydrogen aerosol with a high flux of thermal radiation. Finally, a summary of aerosol properties measurements is presented.

Investigation of Aerosol Absorptivity

The effect of each of the four phenomena which dominate the observed experimental behavior is clearly exhibited in Figure 8. These oscillograph traces show the results of He-TaC Test No. 120 202. The top curve shows the combined effect of time variations in the wall and aerosol transmittance, as measured by a laser beam passing through a diameter. The center curve shows the gas pressure time variations as the helium-tantalum-carbide aerosol is heated by the fraction of the available radiant energy which it captures. The lower curve indicates the rate at which thermal radiation strikes the test cell (not the aerosol).

For the first millisecond after triggering the flash (as shown in Figure 8), flash power and aerosol temperature are low. The transmittance

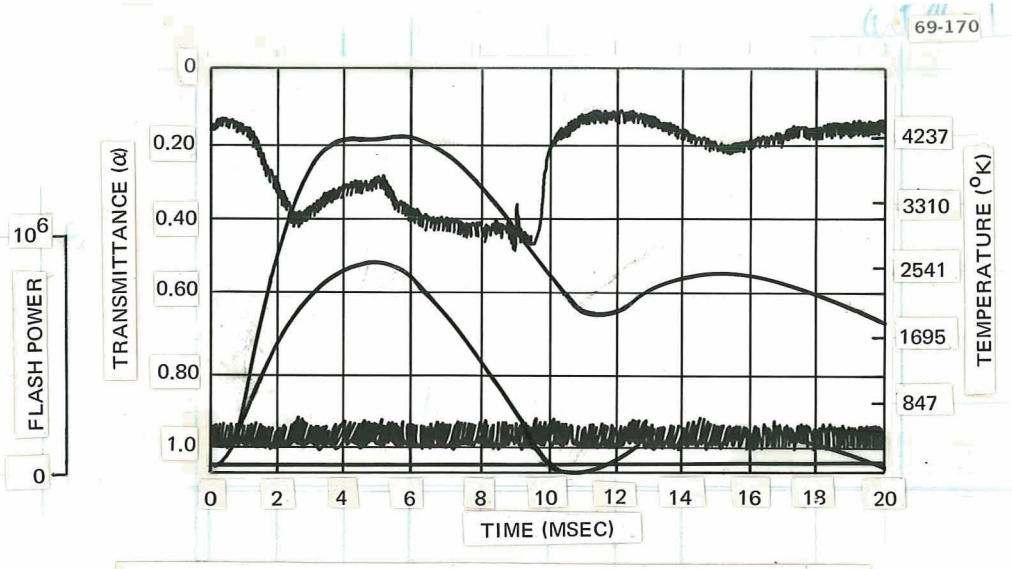

Figure 8. Oscillograph of Results from Test 120202

remains constant and the experimental behavior is described by Equations 29 and 30 for radiant heat transfer to an aerosol.

After the gas has been heated to approximately 1000°K, the appreciably hotter particles begin to evaporate, increasing the measured transmittance. This phenomenon is observed in almost all experiments. That this increase in transmittance is evaporation is substantiated by several observations.

(1) When the aerosol is not flash heated, no such change in transmittance is observed.

(2) A comparison of the flash power observed inside and outside of the flash tube during this time showed no change in the wall transmittance.

(3) When a thin sheet of quartz was placed in the test chamber before flashing, the observed change in transmittance during this time decreased.

Because the wall surfaces were doubled while the aerosol was, to some extent, locally shadowed, this result indicated the wall was not a factor.

(4) An aerosol using aluminum particles which have a lower boiling point showed a greater rate-of-increase in transmittance.

(5) Two-mil foil and 10-mil wires of tungsten and tantalum are easily evaporated at this flash power, and therefore, it is reasonable to assume that those particles fully illuminated by the flash are evaporated.

(6) After the test, the film of particle material on the wall appears to be an evaporative coating, not deposited particles (Figure 9).

Particle evaporation, while extensive, is not complete. A sufficient number of particles remain to absorb (to 5 msec) and radiate (to 11 msec) as is shown by the slope of the pressure curve. Heat transfer rates of this magnitude ($\sim 10^6$ watts) from or to the wall by conduction or convection are highly improbable.

69-171

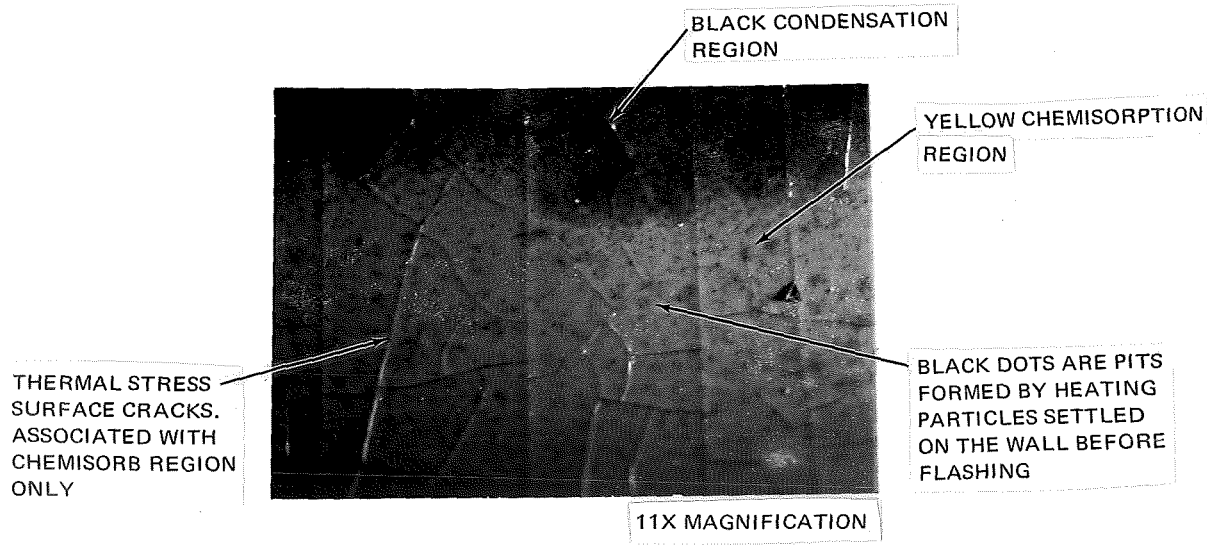

Figure 9. Photomicrograph of Test Cell Inner Surface after Flashing

As evaporation increases the partial pressure of tantalum-carbide vapor in the test chamber (at about 2 msec), chemisorption and condensation occur on the inner wall of the test chamber (Figure 2, Type V). Condensation plays only a minor role at this time because the increased energy absorption on the wall heats the surface, thereby reducing the equilibrium adsorbed layer (ref. 10). Chemisorption, on the other hand, is nonreversible (ref. 10) and the limit on build-up is determined by the number of chemically active sites. That chemisorption is important after 2.2 msec. (Figure 8) is demonstrated by:

(1) Re-flashing the tube after the aerosol has been evacuated returns the observed transmittance to the level ($\alpha \simeq 0.4$ in Figure 8) indicated from 2.2 to 10 msec.

(2) Analysis of the film left on the tube wall after a flash shows the presence of products of a chemical reaction between the quartz and particle material, e.g. silicon metal and copper oxide with copper aerosols.

(3) Surface cracks in the quartz wall (Figure 9) indicate extreme thermal stresses generated by wall energy absorption during the flash.

(4) A dramatic change was observed in the transmittance history and appearance of the tube after the flash when oxides, which will not react with the quartz, were used as particles (Figure 10).

The small decrease in transmittance from 2.2 to 6 msec is ascribed to thermionic emission from the particles, creating an absorbing plasma. This dip is regularly observed in dense aerosols. The only data tending to confirm the existance of this phenomena are measurements of the electrical conductivity of the aerosol during the flash. These measurements showed the aerosols was conductive only for a short time around the maximum of flash power, roughly corresponding to the observed dip in transmittance. Experimental difficulties prevented measurement of the electron number density for numerical comparison with theory. The observed conductivity of ~20 mho/cm is sufficient, however, to argue that an energy absorptive plasma exists.

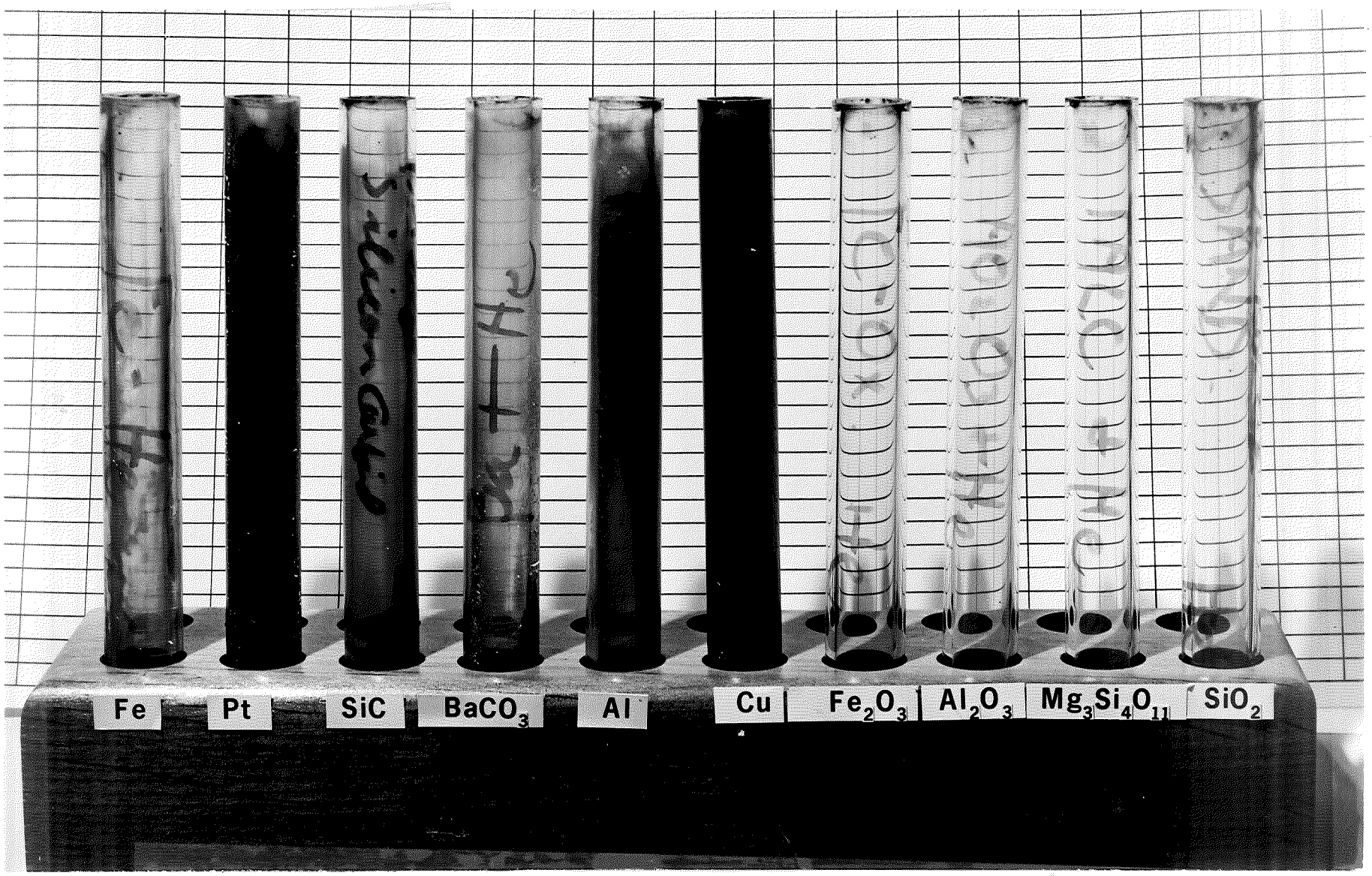

Figure 10. Test Cells After Heating Helium Aerosols Containing the Listed Particle Materials

Shortly before 10 msec in Figure 8, flash power drops to zero and transmittance abruptly decreases. This behavior is ascribed to condensation or physical adsorption of the vaporized particle material onto the wall. This is well supported by:

(1) The reported behavior as shown in Figure 1, with the reasonable assumption that only after the flash power is zero does increased wall condensation not cause increased wall energy absorption and consequently higher wall temperatures.

(2) The transmittance increases (around 16 msec) when the ringing discharge circuit causes a second, smaller flash.

(3) Condensed particle material appears on the test cell wall after the flash (Figure 9).

(4) The observed transmittance decreases when an air-hydrogen explosion is induced in a non-flashed test cell.

In this latter experiment, water condensed on the test chamber wall during the time when pressure was rising as a result of H_2, 0_2 chemical reaction. This showed not only that wall condensation reduces transmittance, but that this condensation is also very rapid and can occur while the vapor is superheated above its saturation temperature.

These experiments demonstrate that the observed low radiant heat transfer rate from the flash tube to the aerosol is caused by the presence of the quartz wall. While the quartz is initially transparent to thermal radiation, chemisorption and condensation reduce its transparency as soon ($\sim$2 msec) as a vapor is available. (No evidence is available one way or the other but there is no apparent reason why hydrogen will not chemisorb on quartz.) Radiant heating probably keeps the wall relatively clear of condensed vapor, but chemisorption appreciably reduces the energy flux to the aerosol. The pressure histories and energy absorptivity observed in the flash heating experiments can consequently be explained by three

phenomena: partial evaporation of the aerosol particles; reduction of the incoming flux by an energy absorbing wall, and radiant heat transfer to a two-temperature aerosol. A fourth phenomena, thermionic generation of a plasma is probably also important.

Figure 11 shows a comparison between experiment and theory, neglecting plasma absorption. The program listed in Appendix C was used to compute the theoretical result. The flux incident on the aerosol was assumed to be the flux from the flash lamp reduced by the theoretical wall transmittance curve shown in Figure 11. The assumed aerosol transmittance changes as a result of evaporation are shown. Figure 11 cannot be considered quantitative verification of theory because the separate wall and aerosol contributions to the total transmittance were assumed, reasonably on the basis of available evidence, but nevertheless assumed. Separate measurements of these two contributions to the total transmittance are extremely difficult but will be necessary for confirmation of the theories.

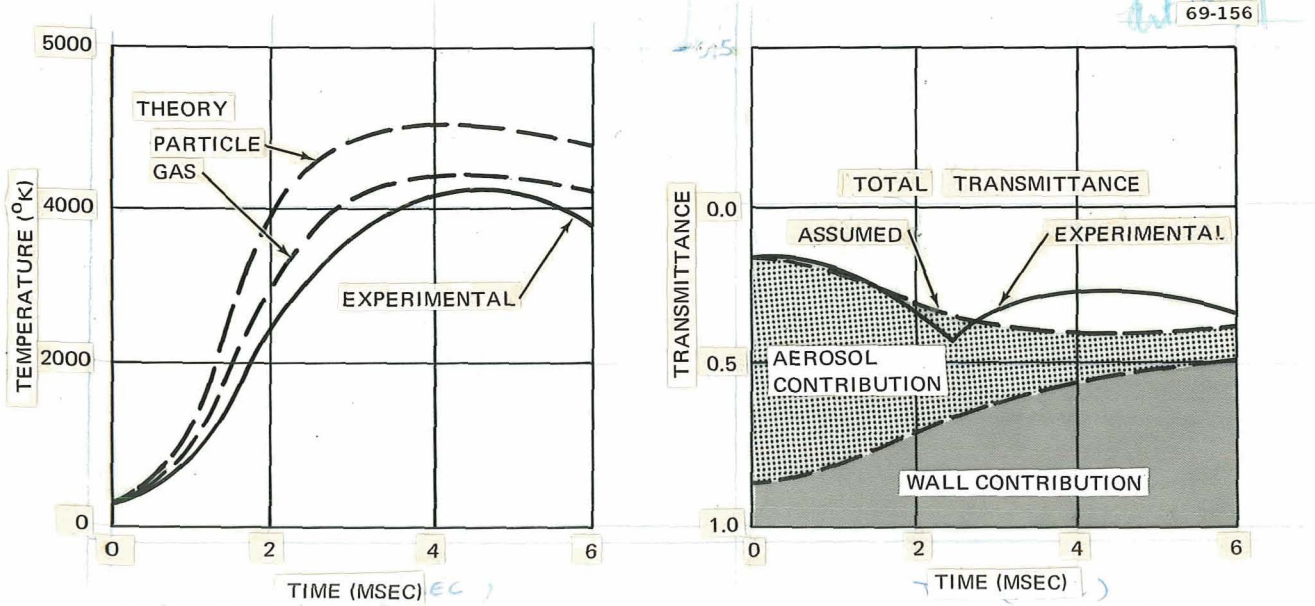

Figure 11. Comparison between Observed and Predicted Helium Temperatures (Test 120202) with Assumed Transmittance Components

Investigation of Maximum Aerosol Temperature

The purpose of these experiments was to obtain the highest hydrogen aerosol temperature possible with the present apparatus and to investigate the mechanisms which limit energy absorption in an aerosol. The first step was to empirically identify the parameters which determine the magnitude of the temperature maximum; the second was to optimize these parameters within the limitations of the experimental apparatus. Achievement of a hydrogen aerosol temperature approaching 6000°K was the goal. Unfortunately, the wall effect prevented achievement of this goal, but a sufficiently high temperature (5300°K) was achieved to indicate that, with more energy per unit mass of hydrogen, there would be no difficulty in reaching 6000°K. However, it is apparently beyond the capability of the present flash-heating technique to achieve the required energy.

Figure 12 shows the successful identification of the most important parameters determining the magnitude of the temperature maximum. Each point represents the temperature maximum in a single test. With a constant flash energy, pulse duration, and shape, and a constant aerosol transmittance and initial pressure, the magnitude of the temperature maximum was reproducible, indicating E, τ, α, and Po are the most important parameters. The error bars on Figure 12 represent the 75% confidence level that 75% of all new data will fall within the indicated limits. These limits were obtained by a least-squares fit of a straight line to the data. The existence of some scatter in the data indicates the presence of undetermined parameters. The scatter is worse at higher flash energies and lower pressures, and is probably a result of non-uniformities in the aerosol producing variations in chemisorption at the wall.

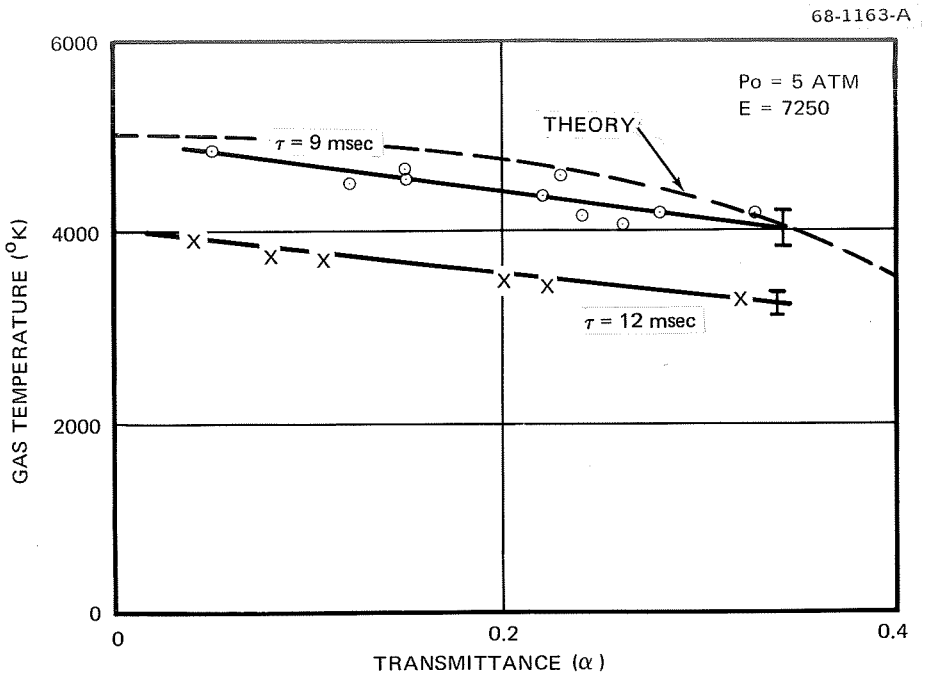

Figure 12. Hydrogen Temperature Maximum Dependence on Initial Optical Transmittance

Figure 12 also shows the experimental dependence of the hydrogen temperature maximum on total, initial transmittance. The broken line shows the dependence predicted by radiant heat transfer theory, assuming the walls remove a sufficient, constant fraction of available flash energy to produce the temperatures observed. Equation 7 was used to relate transmittance and the fraction of energy absorbed. The observed and predicted shapes agree reasonably well, indicating at least a qualitative confirmation of theory.

A plot similar to Figure 12 was required for each set of the parameters. flash energy, E, flash duration, τ, and initial pressure, Po, because the aerosol transmittance, α, could be controlled experimentally only within, $\pm 100\%$. Determination of a constant α surface in the four-dimensional parameter space required, therefore, a set of measurements at each E, τ, and Po, followed by interpolation of the data to establish the value of the

hydrogen temperature maximum expected at a given α. This procedure was followed for five total-flash energies from 1800 to 7240 joules, four flash durations from 2.2 to 12 msec, and four initial hydrogen pressures from 1/2 to 5 atmospheres.

Figure 13 shows the effect of increased flash duration on the hydrogen temperature maximum. Each point and its associated 75%-75% error bars is an interpolation of 3 to 10 measurements over a range of transmittances. At low flash energies, the effect of flash duration on aerosol temperature is smaller than at high flash energies. Qualitatively, this is reasonable because, high flash energies cause higher gas and particle temperatures which increases the rate of radiant energy loss from the aerosol. Therefore during the longer flash duration, a larger percentage of the absorbed energy is reradiated by the aerosol before the gas reaches its peak temperature.

Figure 14 shows the results of an energy survey. Again, each point represents interpolations from 3 to 10 tests. The abscissa is the flash energy available up to the time when the maximum gas temperature occurs.

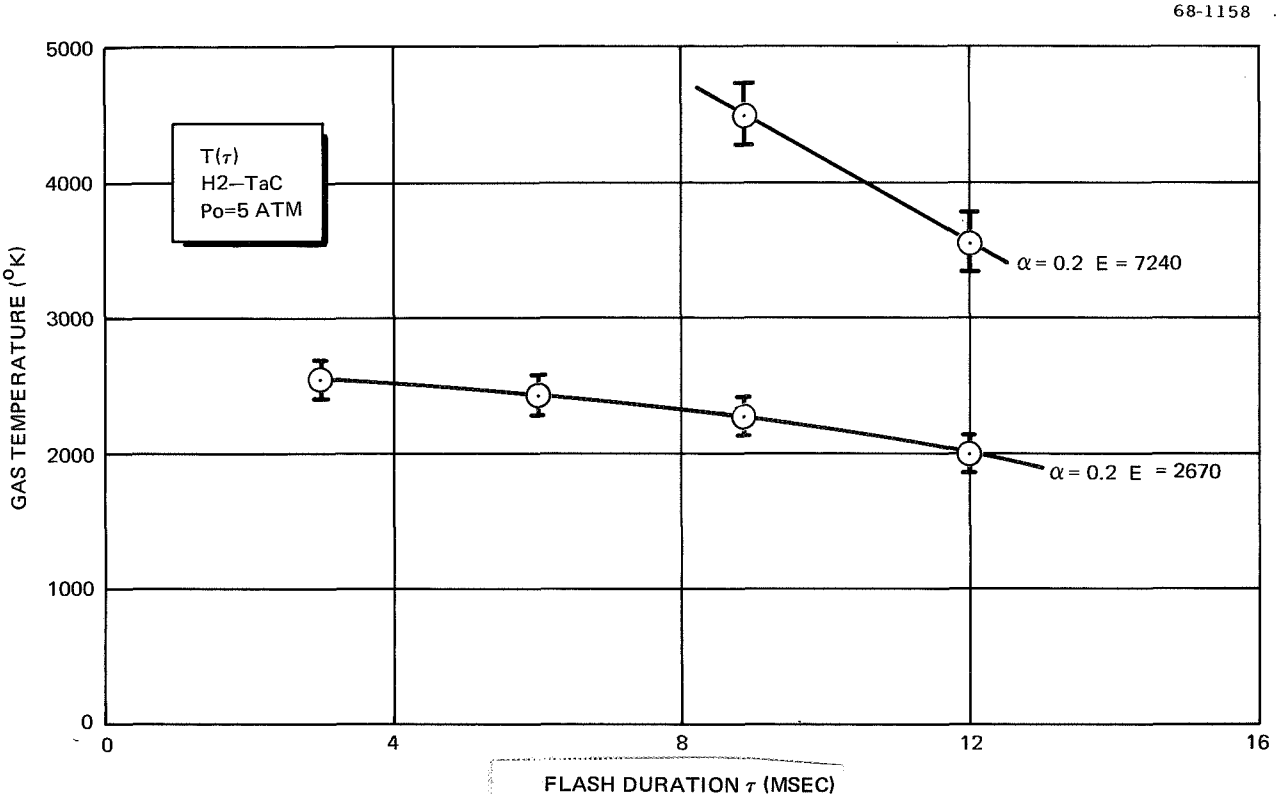

Figure 13. Hydrogen Temperature Maximum Dependence on Flash Duration of Two Flash Energies

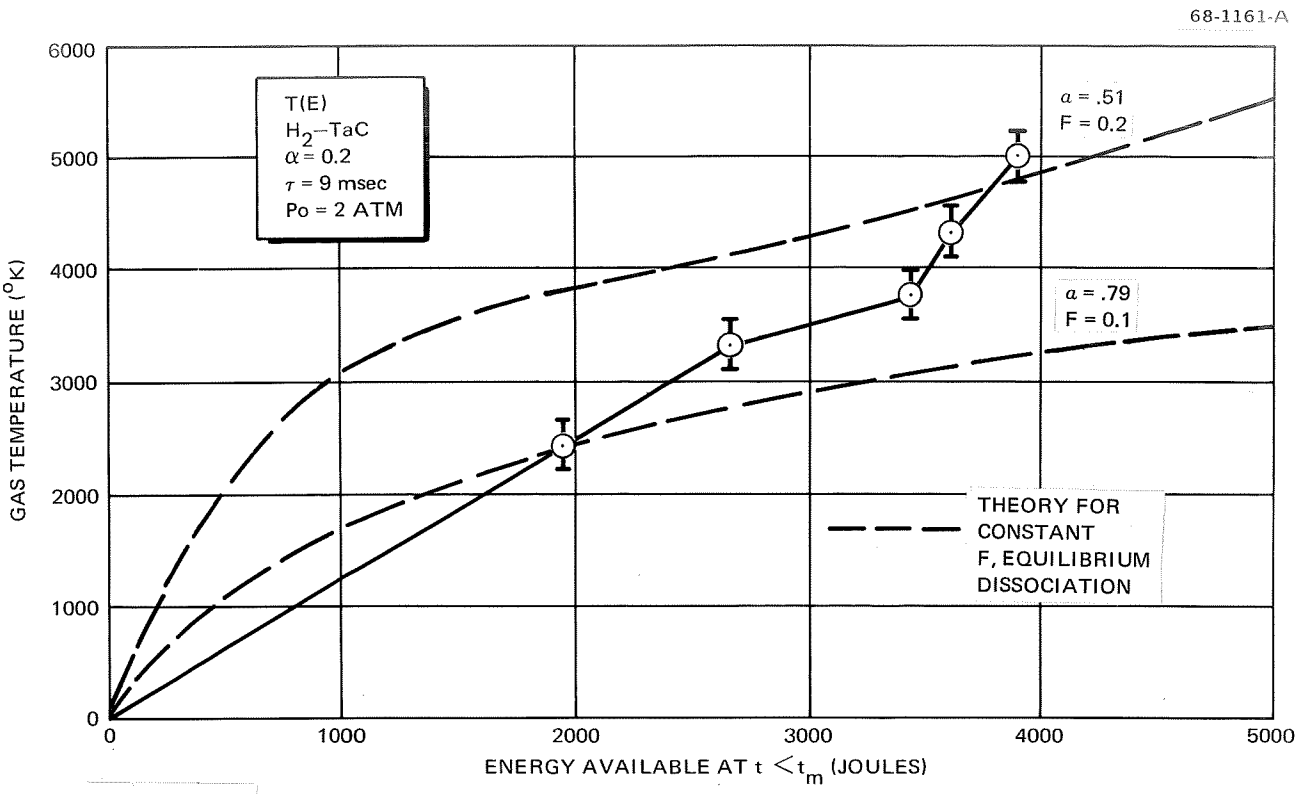

Figure 14. Hydrogen Temperature Maxium Dependence on Flash Energy Available to the Aerosol up to the Time of the Gas Pressure Maximum

This energy (about 60% of total flash energy) was chosen as the coordinate to eliminate any bias introduced by the shape of the underdamped flash pulse (Figures 15 and 16) at the longer flash durations. The maximum flash energy available to the aerosol (7240 joules) exceeded expectations but is still not sufficient to produce a hydrogen aerosol temperature above 6000°K.

The low energy absorptivity of an aerosol at the high flux and temperatures achieved in the flash-heating experiments is shown by a comparison between predicted and experimental results (Figure 14). The theoretical curves (broken lines) are based on the assumptions that the same fraction, F, of the available flash energy is absorbed by the aerosol as the available energy is increased, and equilibrium hydrogen dissociation occurs at the aerosol temperature. The slope of these curves would be further reduced by radiation loss from the aerosol. Two contradictions are apparent.

69-168

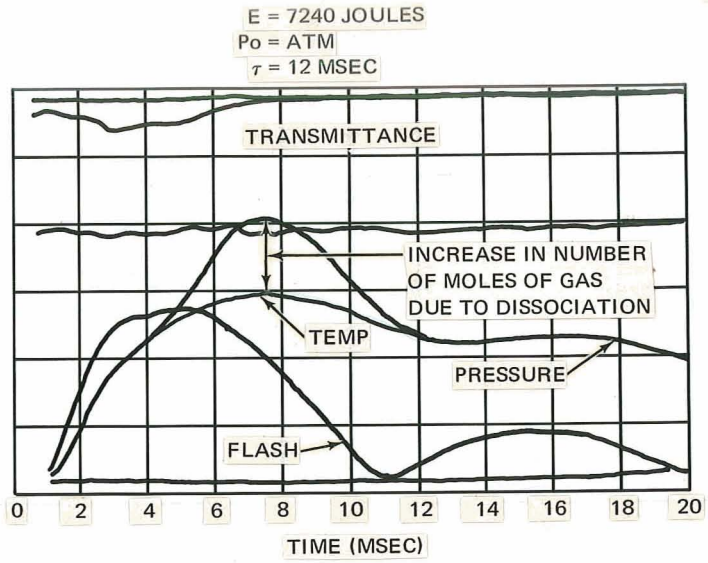

15

Figure 15. Hydrogen Test 062501

69-169

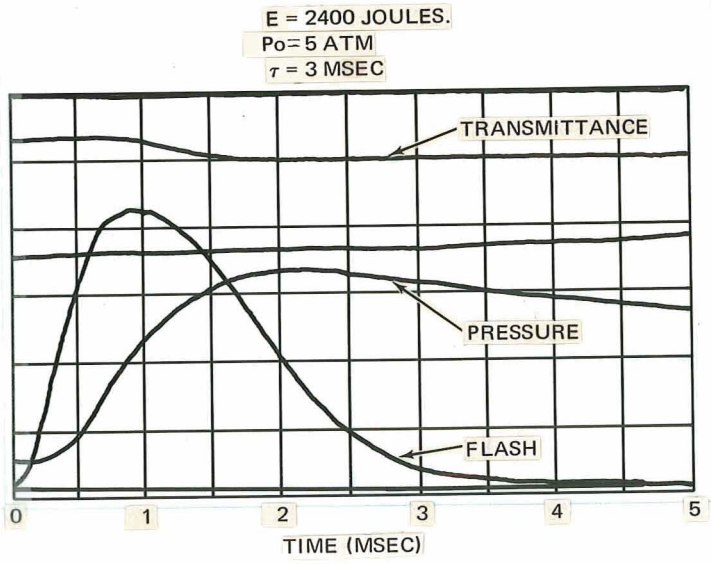

16

Figure 16. Hydrogen Test 053101

First, the experimental temperatures roughly correspond to what would be expected with aerosol transmittances ~0.6, instead of the more dense aerosol transmittance of 0.2 which was measured. Second, at these energy adsorptivities, only a small increase in temperature is expected with increasing energy as soon as the hydrogen dissociation temperature is achieved. Well-verified experimental results, in contrast, show a leveling off, followed by a sharp increase at temperatures considerably lower than required for complete dissociation.

The raw data for high and low energy flashes (Figures 15 and 16) explain this discrepancy. At a high flash energy, the transmittance trace shows that wall sorption blocks the flash energy from reaching the aerosol well before the temperature maximum is achieved. The actual energy available to the aerosol is considerably less than indicated on the abscissa of Figure 14. In contrast, appreciably less wall sorption is indicated by the transmittance trace in Figure 16. A greater fraction of the flash energy penetrates the wall and is available to the aerosol. The discrepancy between theory and experiment indicated in Figure 13 is consequently the result of uncertainty in assigning each data point to the proper abscissa.

A similar discrepancy is shown in Figure 17. Doubling the initial pressure doubles the amount of hydrogen gas and, modified by dissociation, roughly doubles the heat capacity. The experimental dependence of the hydrogen temperature maximum on initial pressure is consequently expected to be much greater (broken curve) than observed. As shown in the raw data for a 1/2-atm test in Figure 18, in contrast with the 2-atm initial pressure test of Figure 15, the pressure maximum exhibits a flat top. Studies with helium-tantalum-carbide aerosols (Figure 8) have established that this phenomena is associated with a marked decrease in the energy absorbed by the aerosol resulting from either (or both) particle evaporation and wall sorption.

Figures 19 and 20 summarize the optimization procedure used to find the set of values of E, τ, P_o, and which limit the maximum hydrogen temperature obtained with the present apparatus. This limitation exists

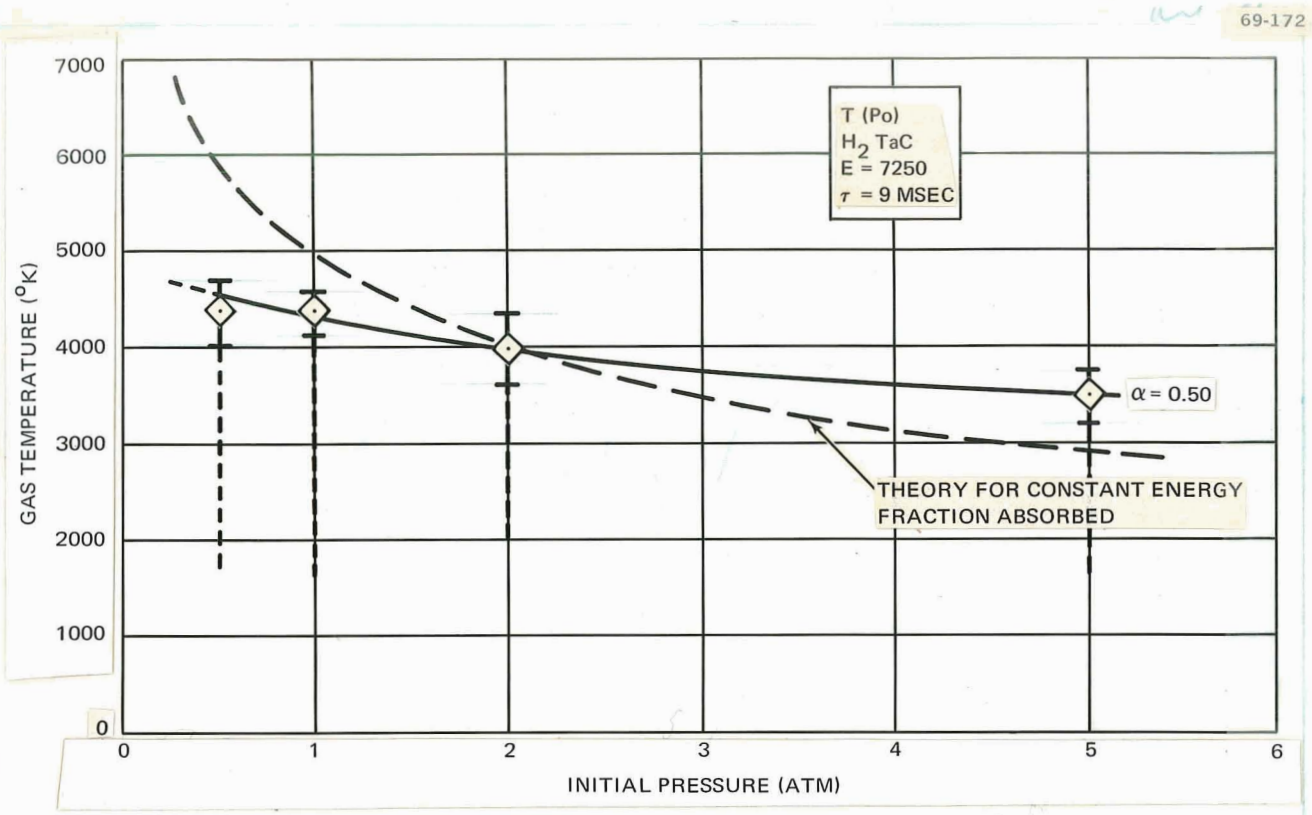

Figure 17. Hydrogen Temperature Maximum Dependence on Initial Pressure

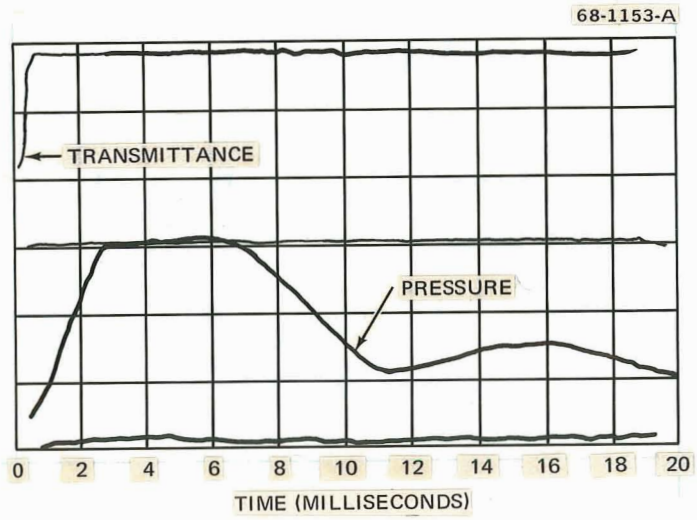

(NOTE: TRANSMITTANCE MEASUREMENT INVOLVED AFTER O MSEC)

Figure 18. Raw Data for H_2–TaC Test Number 072423. (Initial Pressure, ½ atm)

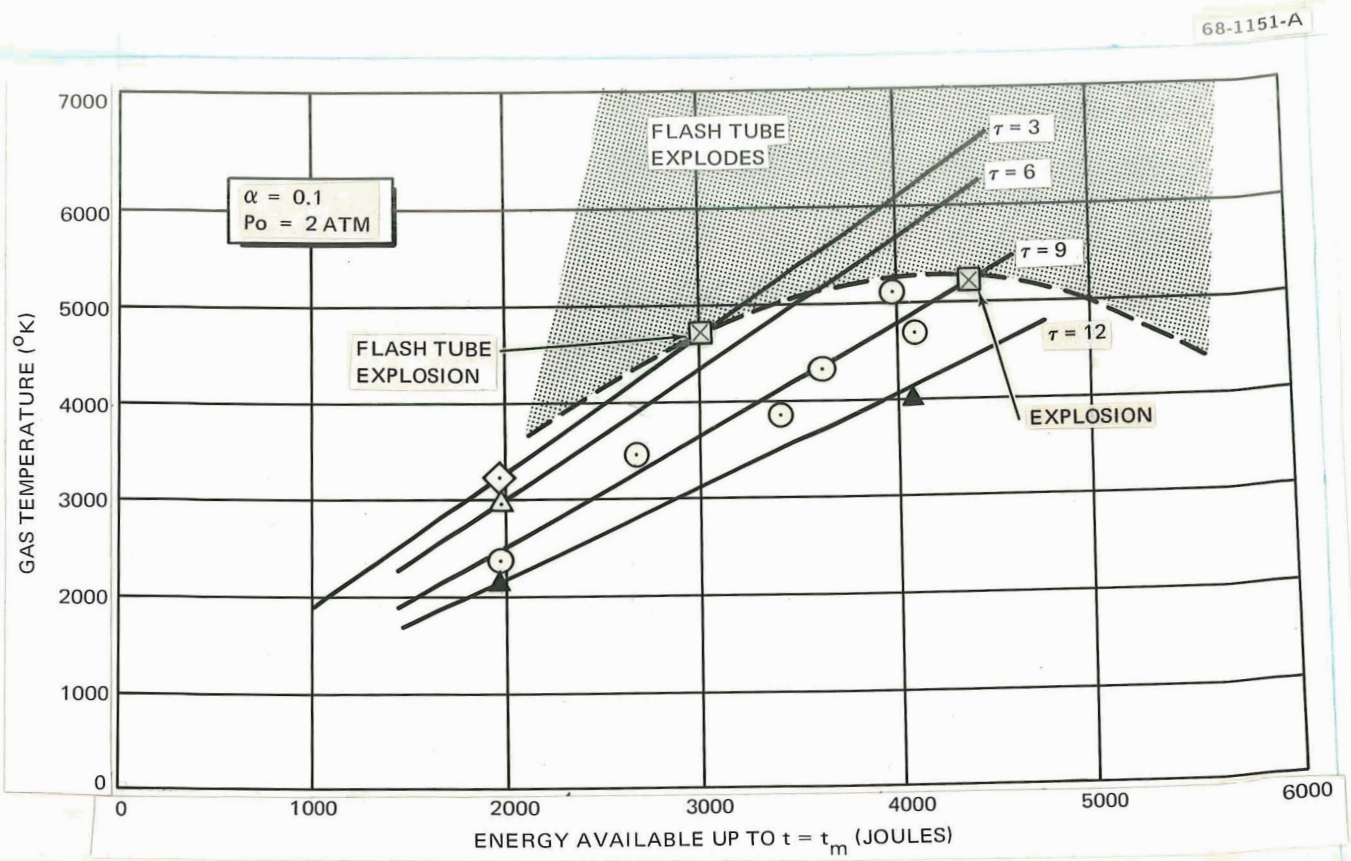

Figure 19. Energy, Temperature and Flash Tube Explosion Limit Relations

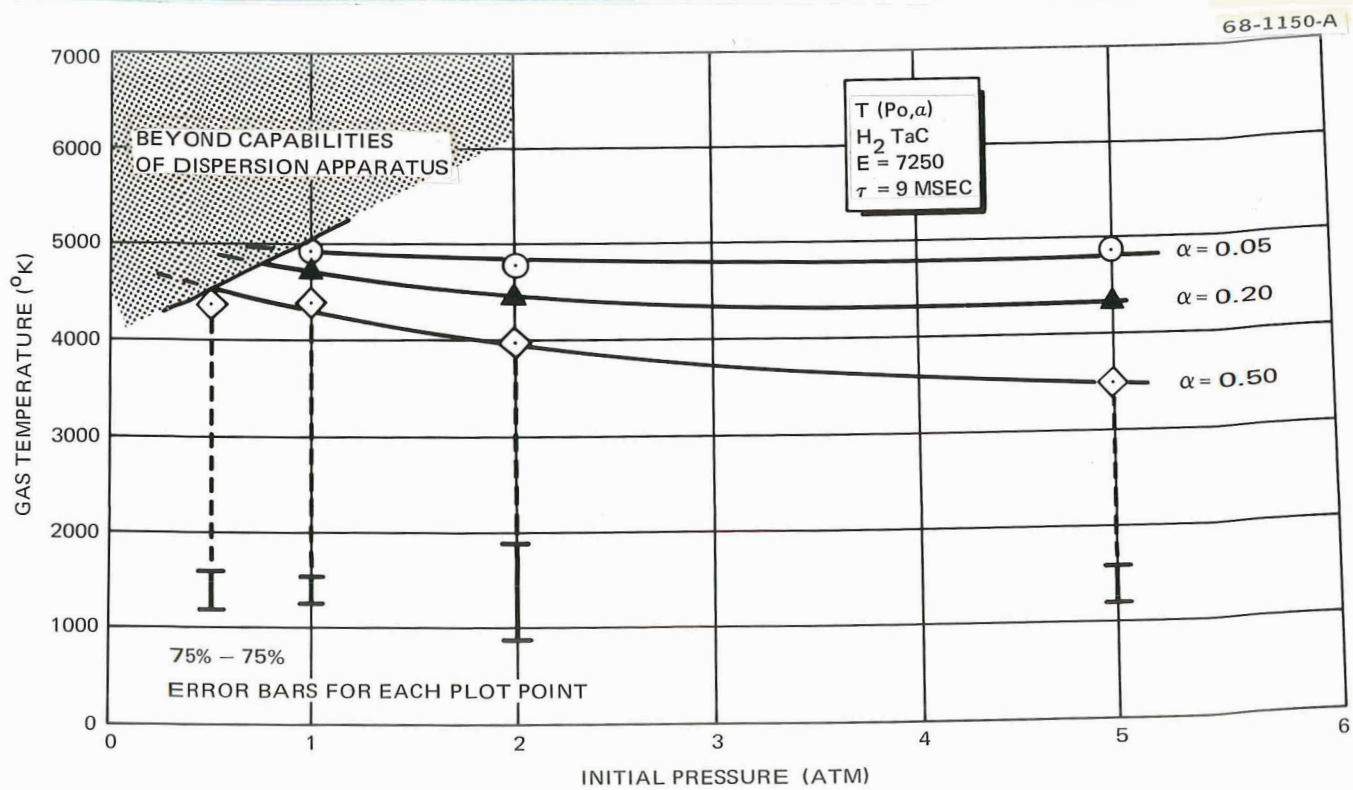

Figure 20. Initial Pressure, Optical Transmittance, and Temperature Relations

because of flash tube explosion and aerosol dispersion limitations in the apparatus. Figure 19 indicates that maximum gas temperature is achieved with 4500 joules of available flash energy in a 9-msec flash. Shorter flash durations at the same energy or higher energies at the same flash duration (shaded area) cause the flash tube to explode, while the converse results in lower gas temperatures. Figure 20 indicates an optimum at 1 atmosphere initial pressure with an optical transmittance of 0.05. The unavailable region shown on the left by shading is a consequence of less gas carrying fewer particles into the test cell, which results in a higher transmittance and less energy absorption. Alpha equal to 0.05 represents a very opaque aerosol and is the maximum available with the dispersion apparatus.

The survey of helium-tantalum-carbide aerosols was not as extensive. These tests were used to check the hydrogen results by using an ideal, nondissociating, chemically inert gas with a high ~12 000°K ionization temperature. Table 1 lists the temperature maxima for 15 of the helium tests. As shown in Table 1, even without the optimization procedure used with hydrogen, higher maximum temperatures were achieved because of the lower helium heat capacity. All observed phenomena, except dissociation, were common to both helium and hydrogen.

The principal value of the helium aerosol tests was that they exhibited that a tantalum-carbide aerosol contained in a quartz cylinder can be heated to above 6000°K with a flux of ~40 kw/cm^2. This suggests that any limitation in hydrogen aerosol temperatures is not caused by particle evaporation alone.

Aerosol Properties

The properties of the aerosol formed by the flash-heating dispersion apparatus were extensively studied. Experience and theory both indicated these properties are very important in radiant heat transfer to an aerosol.

TABLE 1
SELECTED HELIUM-TANTALUM CARBIDE TEST RESULTS

Maximum temperature, °K	Flash energy, J	Flash duration, μ sec	Initial pressure, atm	Optical transmittance	Test no.
2336	1212	3	1.8	0.93	0319-07
3237	1212	3	1.8	0.66	0321-07
4210	1212	2.5	1.8	0.62	0327-02
3434	1212	2.5	4.9	0.27	0327-04
2742	1212	2.5	10.0	0.22	0327-06
4047	1212	2.5	2.2	0.37	0410-02
4844	1212	2.5	1.8	0.16	0422-03
5858	3309	3	1.9	0.18	0426-02
3125	3309	14	1.9	0.23	0426-03
3476	4400	14	1.9	0.23	0426-06
6597	4667	2.5	1.8	0.34	0423-02
6082	2959	2.5	1.8	0.14	0423-07
5702	3333	3.0	2.0	0.16	0820-05
5702	3600	3.0	2.0	0.23	0820-04
5302	3333	3.0	2.0	0.29	0820-02

The results of particle-size measurements by two techniques are summarized in Figures 21, 22, and 23. As shown in Figures 21 and 22, the electron photomicrographs indicate an average particle radius of about 0.1 micron. A correlation of experimental measurements of mass dispersed and transmittance, however, indicated appreciable agglomeration. Based on Equation 6 and an assumed agglomerate density of 1/3 that of tantalum carbide, the agglomerate particle radius is about 2 or 3 microns.

A comparison between the energy absorptivity early in the test and the measured transmittance tends to confirm the aerosol property theories discussed under Quartz Wall Sorption. Figure 24 shows the energy absorptivity (ratio of power-to-the-gas to the radiation power available) varies with time as determined from the slope of the pressure curves (Appendix B). The initial rise is a measure of the delay in transferring energy to the gas from the particles and shows that the time of the system is short compared with

68-1157

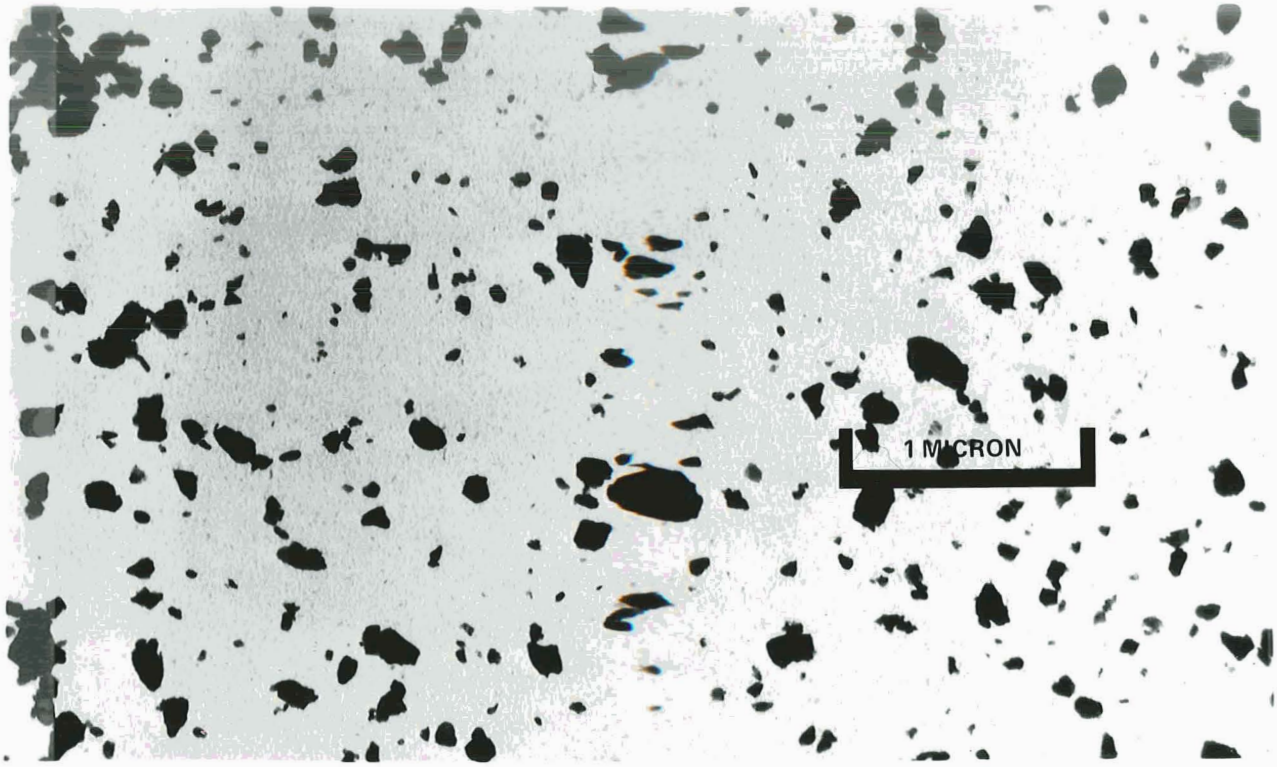

Figure 21. Electron Micrograph of Tantalum Carbide Particles

68-1162

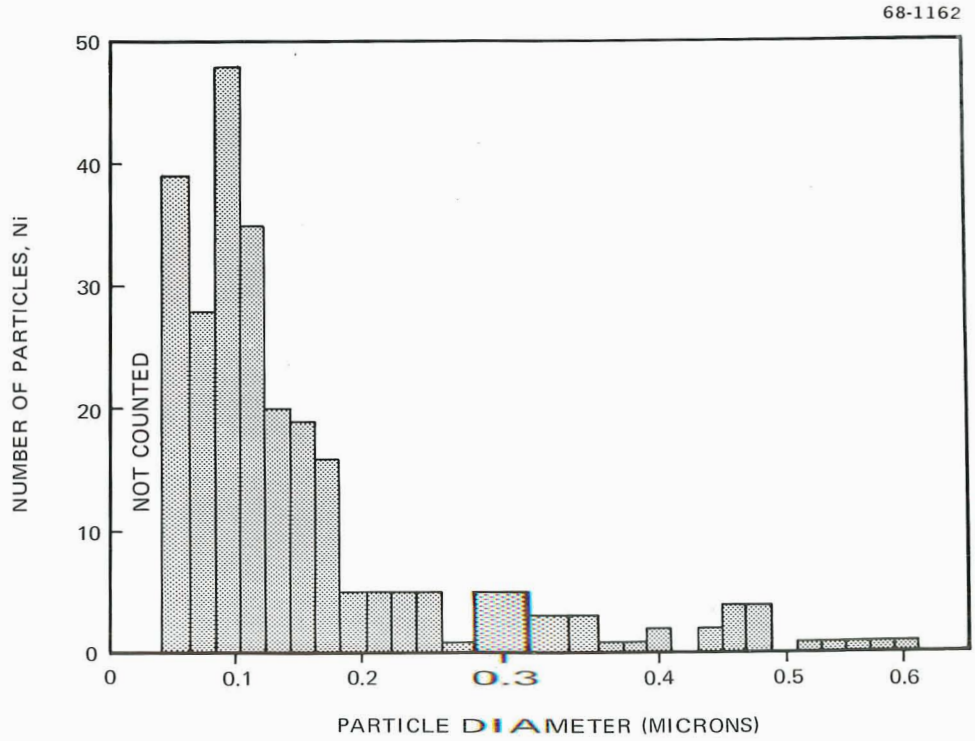

Figure 22. Tantalum Carbide Particle Size Distribution

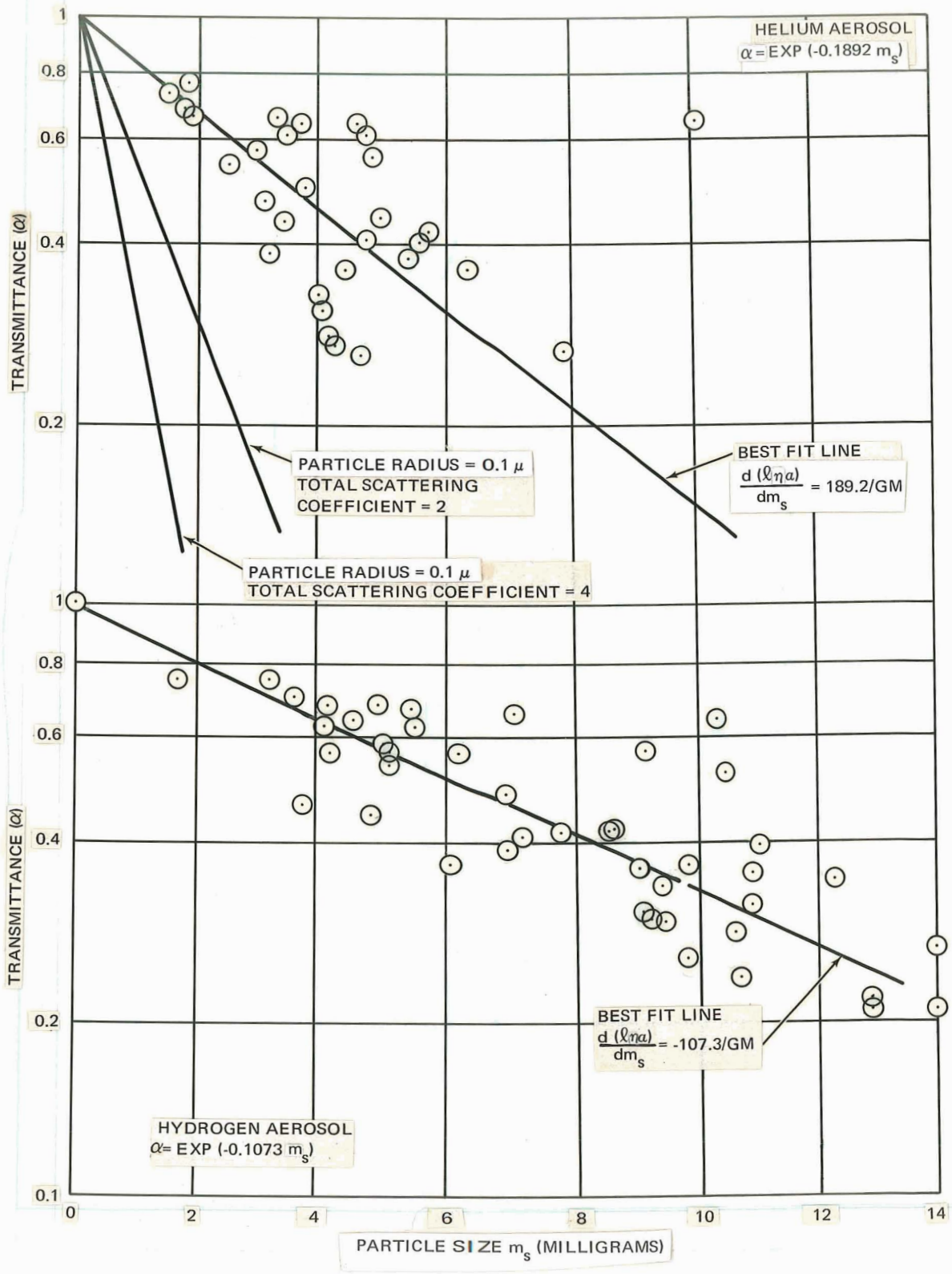

Figure 23. Beers Law Correlation of Aerosol Properties

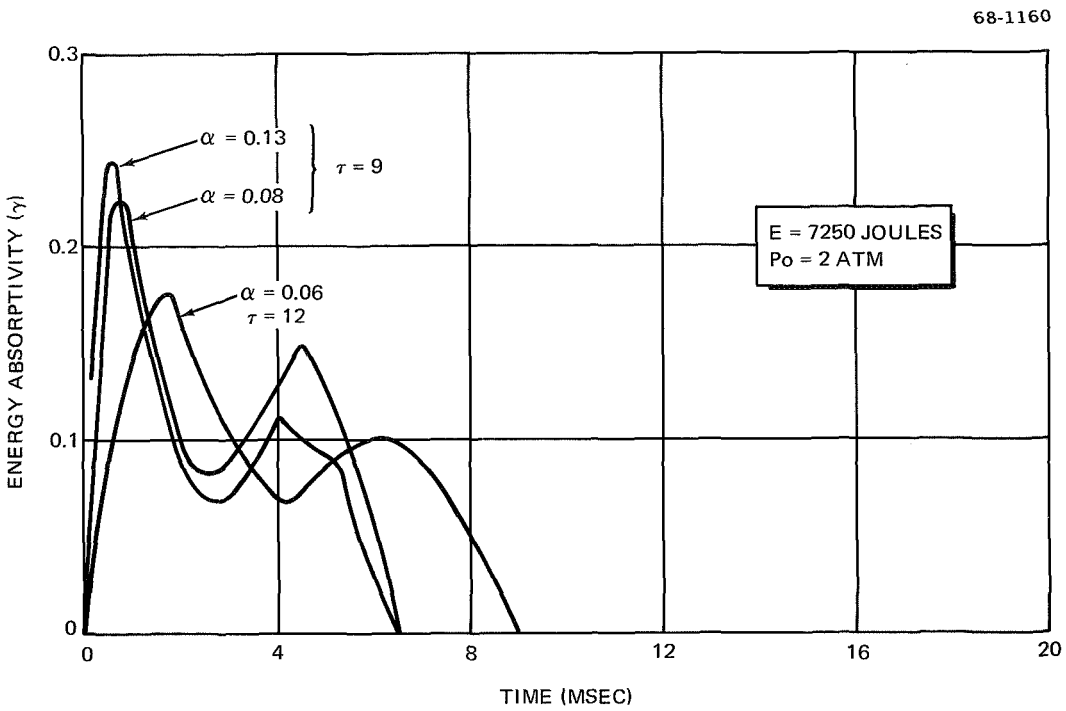

Figure 24. Fraction of Available Energy Absorbed in the Gas, γ, as a Function of Time

the flash duration. At the top of the first peak, energy is being transferred to the gas as rapidly as it is being absorbed by the particles. Particle temperature is also still sufficiently low so that reradiation losses are not important and wall sorption is at a minimum. This peak, therefore, gives the energy absorptivity of the particles, γ_o.

After the γ_o peak, particle temperature continues to increase and radiation losses from the particle become appreciable, and γ, the energy absorptivity of the gas, decreases even if the fraction of available energy absorbed by the particles, γ_o, remains constant. Wall sorption also reduces the energy available to the aerosol. The second peak shown in Figure 24 is probably a result of increased plasma absorptivity.

After the second peak, γ falls monotonically to zero at the pressure maximum. At this time, the energy loss rate equals the energy input rate to the aerosol. This point and similar points, where the pressure is a

maximum or minimum (Figure 8), can serve as a check on the assumed energy loss and absorption mechanisms. For example: If reradiation resulting from gas temperature causes the only heat loss, the particle emittance and surface area cancel out, and the radiation from the aerosol, $A_w \sigma T_p^4$, should equal the available flash power. A comparison of these numbers, for a typical test, show the wall is absorbing energy at a rate of ~300 kw, because the incident power is ~700 kw while the radiated power at the maximum gas temperature is ~400 kw.

Figure 25 shows a comparison between the energy absorptivity of the particles, γ_o, as determined above and the optical transmittance, α. If the scattering contribution to α was constant, these data would generate a curved line passing through the origin according to Equation 7. The actual data are scattered, indicating either the initial peak of γ is not consistantly the energy absorptivity of the particles or inaccuracies in measuring α.

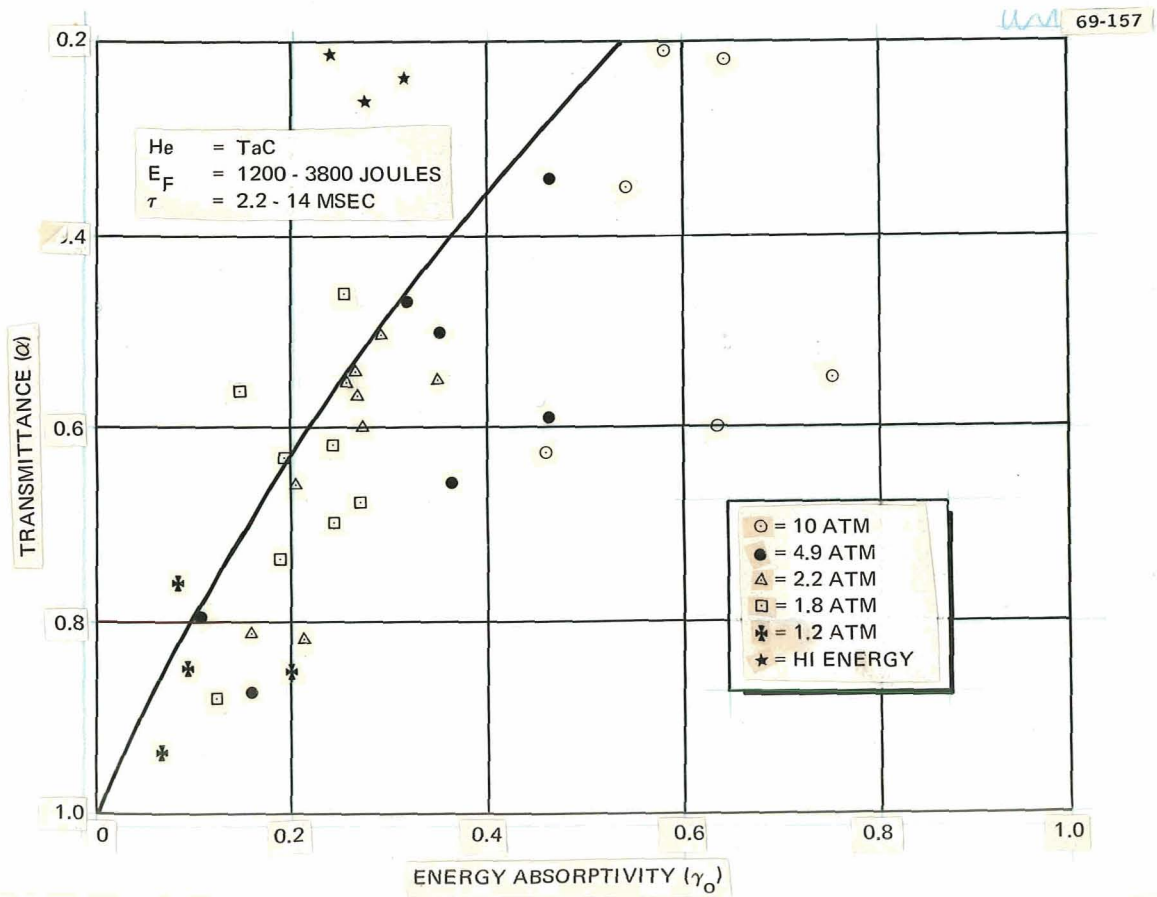

Figure 25. Experimental Relation between the Energy Absorbitivity of the Particles (γ_0) and Optical Transmittance (α).

RESULTS AND CONCLUSIONS

1. Aerosols of tantalum-carbide and hydrogen, contained in a quartz wall, can be flash heated to temperatures of 5300°K. Nothing was found during this program that indicates that these temperatures would not be attainable in a nuclear propulsion system using the seeded-gas concept.

2. The analytic model used to correlate experimental results required inclusion of aerosol reradiation and wall effects before general agreement with observations was obtained. With the inclusion of wall effects qualitative interpretation of experimental results was possible. However, quantitative evaluation of wall phenomena has not yet been achieved.

3. In propulsion systems where transparent partitions are proposed, consideration must be given to chemical compatibility of the aerosol with the partition. The interpretation of wall interaction in the flash heating experiments must be understood to be speculative and without strong confirming evidence. However, generally satisfactory agreement between experiment and theory was obtained only after appropriate representation of the wall effect was included in the analytical model for flash heating experiments.

4. Measurable electrical conduction does occur in a hydrogen-tantalum carbide aerosol as a result of exposure to a high radiant flux ~40 kw/cm^2, indicating production of a significant level of ionization.

Donald W. Douglas Laboratories
McDonnell Douglas Astronautics Company - Western Division
Richland, Washington, February 7, 1969

Page intentionally left blank

Appendix A

FLASH HEATING EQUIPMENT AND PROCEDURES

The basic flash heating apparatus is shown in Figures A-1 and A-2. The apparatus consists of four parts: (1) the energy-storage capacitors, 1A charging power supply, 1B, and pulse shaping inductors, 1C; (2) the time delay panel, 2A, flash-tube trigger circuits, 2B, and spark gap switch circuitry, 2C; (3) the elliptical reflector, 3A, flash tube, 3B, and test cell, 3C; and (4) the gas gottles, 4A, surge tank, 4B, gas solenoid valve, 4C, and particle dispersion apparatus, 4D.

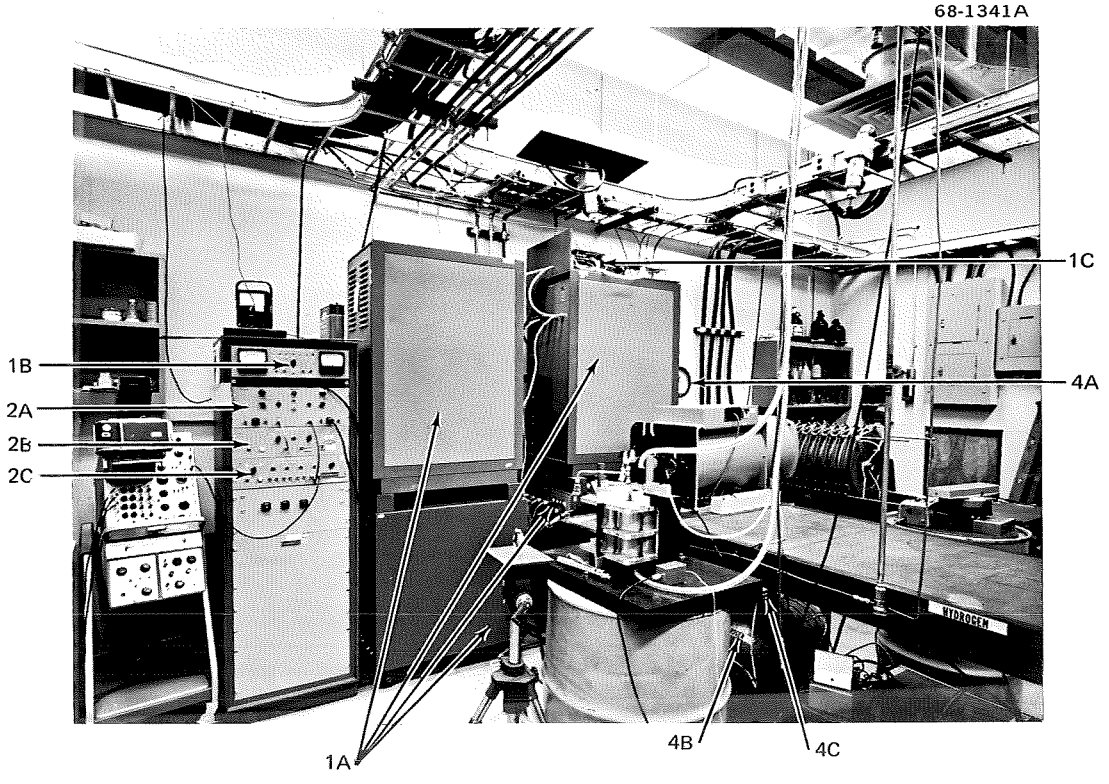

Figure A1. Flash Heating Experimental Apparatus

68-1339A

Figure A2. Elliptical Reflector, Flash Lamp, and Test Cell

To flash heat an aerosol, a measured quantity (50 to 450 mg) of tantalum-carbide powder is placed in the dispersion apparatus. The pressure-regulating valve on the gas bottle (4A) is set to the desired initial pressure as indicated on a Heise Model C-54011 pressure gauge, and the surge tank (4B) is filled with gas. The Skinner Electric Model V520A1200 gas solenoid valve (4C) is closed. The test cell (3C), dispersion apparatus (4D), and the gas line to the solenoid valve is evacuated to less than 10 torr and isolated from the vacuum pump. Four 960-mfd, hv Model 1210 CMI energy-storage capacitors (1A), are charged to the desired voltage, as indicated by a Model 260 Simpson meter.

A switch on the time-delay panel is then depressed initiating the following sequence of events:

(1) The gas solenoid valve opens allowing gas to enter the dispersion apparatus, form an aerosol with the powder, and enter the evacuated test cell through a check valve.

(2) After a selected time delay of ~200 msec, aerosol pressure in the test cell is within 0. 5 psi of surge tank pressure, the check valve closes, and the EG&G Model GP30B spark gap switch (near 1C) is triggered, applying capacitor voltage to the flash tube (3B).

(3) Exactly 0. 3 ms later, the hν Model 1210 TG-4 flash-tube trigger (2B) applies a 20 000-volt pulse to the EG&G FX-47C flash tube (3B).

(4) Current flows from the energy storage capacitors through the inductors (choice of 0. 14, 0. 72, or 4. 6 mh), spark-gap switch, and flash tube which converts approximately 50% of the stored electrical energy to a flash of thermal radiation, at a rate up to 10 megawatts.

The light flash generated at one focus of the elliptical cavity is reflected onto the aerosol contained in the 17 x 1. 28 cm ID test cell at the other focus. A fraction of the light, depending on the optical density of the aerosol, is absorbed by the particles. The particles are heated and some energy is conducted from the particles to the gas. The heated gas is all contained in the test cell by the check valve so that the pressure increases, giving a measure of the temperature and energy absorbed by the aerosol.

Instrumentation was designed to measure aerosol temperature and those properties of the aerosol and thermal radiation field which were believed to determine aerosol temperature. On this basis, instrumentation was developed to measure eight parameters: aerosol pressure, thermal radiation power, and optical transmittance determined as a function of time during the flash; the initial pressure measured just before the flash for each flash test; and auxiliary measurements of aerosol uniformity, mass of particles dispersed, particles size distribution, and total flash energy obtained in separate blank tests.

AEROSOL PRESSURE (P)

The time-resolved aerosol pressure, P, is used to calculate the aerosol temperature history. It is measured with a Kistler Model 613M102 piezoelectric pressure transducer. The pressure-sensitive face of the transducer forms the bottom of the test cell. A loose-fitting metal cap is required to shield the surface from heating by direct exposure to the flash. Output from the transducer is converted to a voltage proportional to pressure by a Kistler Model 566 amplifier, and this voltage is applied to the Y-axis of a Tektronix 549 Memory oscilloscope. Polaroid photographs of the scope face give a permanent record of the time-resolved pressure.

Precision of the system is better than 1% and response time is less than 5 msec. The system is calibrated at 50-lb intervals from 0 to 1000 psi with a Twin Seal Type R100 dead-weight pressure-test unit at least once a month. Because output of the pressure gauge and associated amplifer is linear, a single conversion factor is used in the calculations. After recent difficulties with piezoelectric crystal fracture, the system is also checked, for accuracy in place, once a day, against the Heise Model C-54011 gas-pressure gauge.

THERMAL RADIATION POWER (W)

Time-resolved flash power, W is a measure of the rate at which energy is made available to the aerosol. It is measured with a back-biased SGD100 photo diode with a S1 + S4 response curve. The diode produces an output voltage linearly proportional to the light power over a range of seven decades of incident light and is mounted to remain well within this range by observing

the light from the flash tube through a small hole in the reflector. Response time is less than 0.1 msec. The output of the diode is connected to the Tektronix memory oscilloscope, and Polaroid photography is used to provide a permanent record of the flash power history. The flash curve is calibrated in power units for each test by equating the area under the flash curve ($\int_0^\infty W dt$) to the previously obtained calorimeteric flash energy, E.

AEROSOL OPTICAL TRANSMITTANCE (α)

Transmittance, α, is a measure of the ability of the aerosol to absorb thermal radiation. It is measured for each flash test using the apparatus shown in Figure A3. An Optics Technology Model 170 He-Ne laser (1) projects a monochromatic 3-mm diameter beam through holes in the elliptical

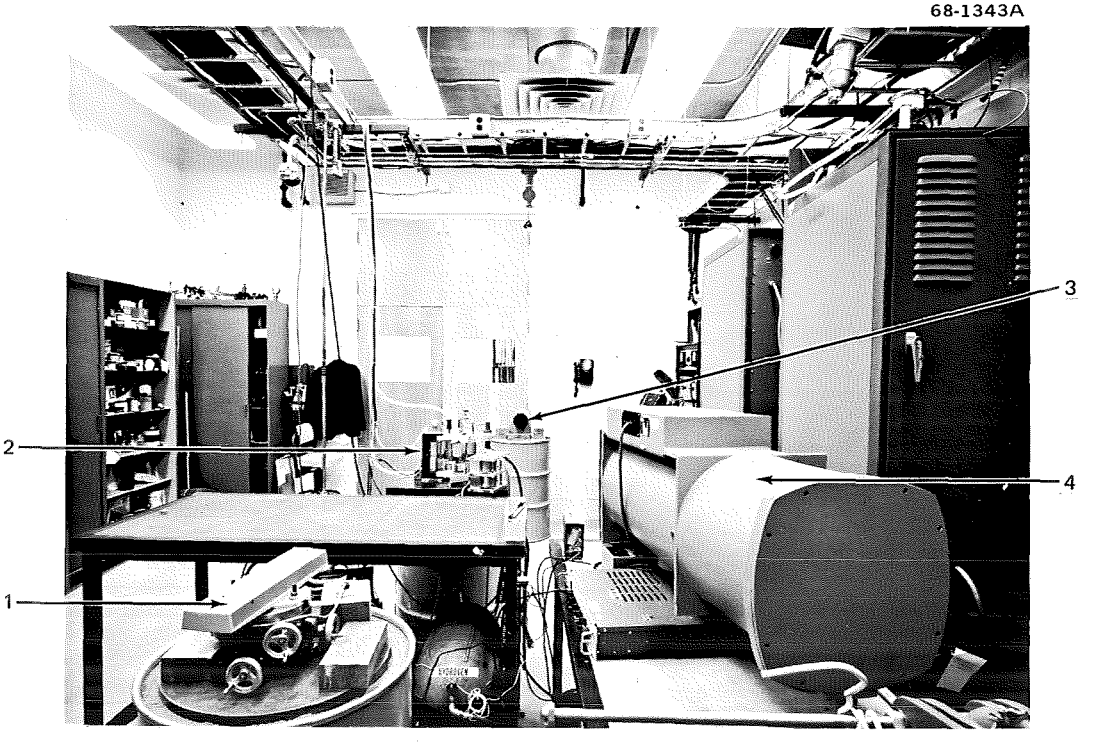

Figure A3. Equipment for Measuring Time-Dependent Optical Transmittance

reflector and through a diameter of the test cell (2). The test cell acts as a cylindrical lens so that the exiting diverging laser beam is focused by a lens (not shown) and a parabolic f9 mirror (3) on the entrance slit of a Jarrell Ash Model 78-492 scanning monochrometer (4). The output of the monochrometer photomultiplier is connected to the memory oscilloscope. The monochrometer and large distances are used to increase the signal (columnated monochromatic, low-power laser beam) to noise (high-intensity, diffuse white light from the flash) ratio. In operation, the blocked, I_o, and unblocked, I_1 laser signal intensity is recorded before the flash to provide $\alpha=0$ and $\alpha=1$ references. The intensity, I, of the signal is then recorded at the beginning and during the flash, and the ratio of $(I-I_o)/(I_1-I_o)$ is the time-dependent transmittance.

The contribution of white light from the flash tube to the measured transmittance was found to be neglibible. This was determined by chopping the laser beam prior to entry into the ellipse and test cell with a rotating slotted disc which produced a chopping frequency of ~4000 Hz. The accuracy of the transmittance before the flash is limited by the readout error of the $\alpha = 0$, $\alpha = 1$, and $\alpha(t)$ traces on the photographs to about ±0.05. During the flash, the explosive flash causes movement of the test cell, laser, and mirror, causing the laser beam to move across the monochrometer entrance slit. The barrels of sand and concrete shown in Figure A3 reduced, but did not eliminate, this source of random noise. This noise caused a ±10% error in measurement of the transmittance.

INITIAL PRESSURE (P_o)

The initial pressure of the aerosol, P_o, in the test cell is a measure of the quantity of gas present and is used to calculate the heated gas temperature and energy content. It is determined by measuring gas pressure in the lines and surge tank (Figure A1, 4A and 4B) with a Heise Model C-54011 pressure

gauge before the gas is introduced into the dispersion apparatus and test cell. The test cell initial pressure at the time of the flash (~200 msec after the solenoid valve admits gas to the test cell) is equal to this line pressure. The Heise gauge is calibrated against a laboratory standard and has a maximum error of 0. 1 psi. Comparisons between the time-resolved test cell and line pressures have established that the 200-msec delay is adequate to allow aerosol pressure to reach within 0. 5 psi of line pressure.

AEROSOL UNIFORMITY [$\alpha(z)$]

Aerosol uniformity is important in obtaining the maximum gas temperature. The axial uniformity of an aerosol is measured by simultaneous determination of the optical transmittance, α, at three axial positions. The equipment, shown in Figure A4 consists of an Optics Technology Model 170 He-Ne laser (not shown), two 1/3 beam spitters and one front surface mirror to split the laser beam into three parallel beams (1), lenses (2) to focus the beams through a test cell (3) (at locations 1/4, 1/2, and 3/4 of the way from the top of the test cell) onto three EG&G SGD 100 photo-diodes (4), a particle-dispersion apparatus (5), the memory oscilloscope, and a Polaroid camera. In operation, the three laser beams are focused to pass exactly through the test cell diameter by superimposing reflections, and the zero ($\alpha = 0$) and 100% ($\alpha = 1$) light levels are recorded on the oscilloscope. The aerosol is then introduced into the test cell, and the transmittance is recorded at the three positions as a function of time. Measured at the center of the tank, the uniformity is ±20% from top to bottom. The basic accuracy of the system is the accuracy of the components, ~2%.

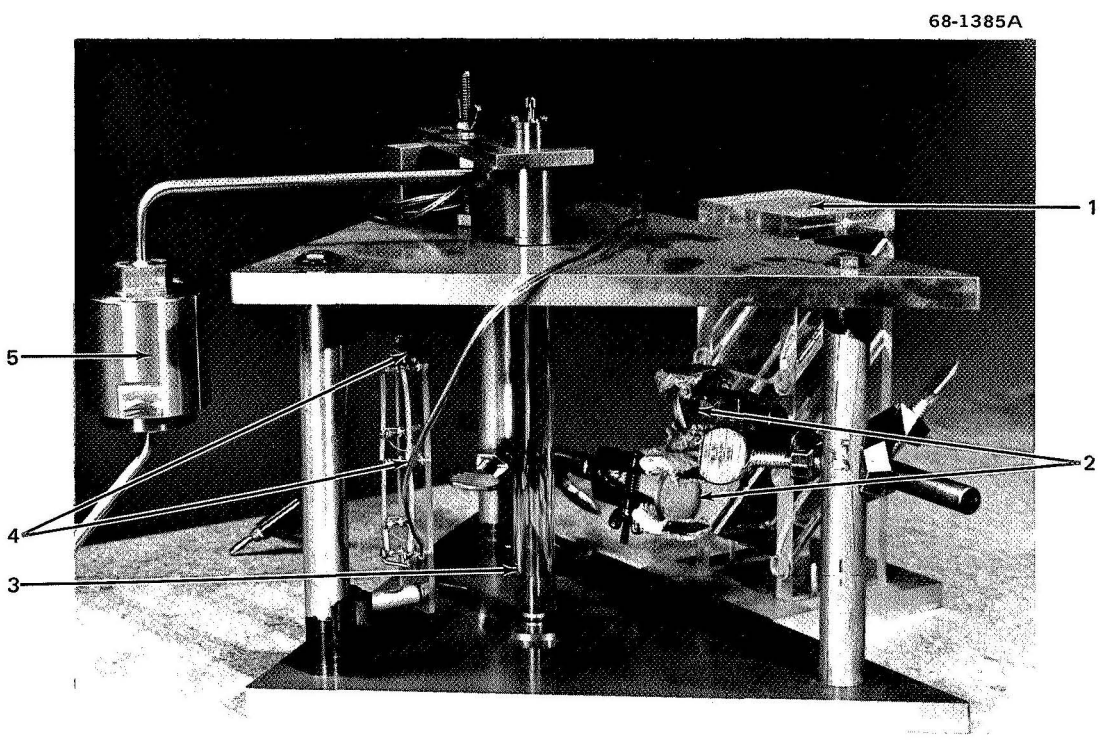

Figure A4. Static Test Apparatus

PARTICLE MASS DISPERSED (m_s)

The mass of particles dispersed in the aerosol, together with the size distribution, determines the optical opacity. Mass is measured using the apparatus shown in Figure A4 and a Mettler Type B6 balance. The tare weight of the test cell, sampling grid, and bottom plug is determined, and the test cell is mounted in the apparatus shown in Figure A4. The aerosol is then introduced into the test cell. After sufficient time has elapsed for all of the particles to have settled out, the test cell and particles are reweighed. The increase in weight is recorded as the mass dispersed, m_s.

Reproducibility and accuracy of these measurements is ±0.5 mg or about 10% of m_s. Achievement of this level of accuracy required considerable

care and the use of electrostatic shields to prevent the charged quartz from affecting the balance.

PARTICLE SIZE DISTRIBUTION (N_i)

Mean particle size and size distribution was determined by collecting a sample of the particle on an electron micrograph grid mounted near the center of the test cell. The grid's surface was parallel to the axis of the test cell. Photographs were then taken of the sample in an electron microscope. These photographs were placed on a Zeiss particle analyzer and a size distribution was determined.

Accuracy of the counting and sizing technique is determined by the experience of the operator. The counting and sizing was done by Battelle Northwest Laboratories in Richland, Washington. The estimated error was ±5%.

Page intentionally left blank

Appendix B
DATA REDUCTION

Extensive calculations are required to reduce raw data to quantities which describe behavior of the aerosol during and after exposure to the high-level radiation field. These data are recorded in the form of Polaroid photographs and numerical values for such parameters as total flash energy and initial pressure. In addition, instrument settings and calibration parameters are available for interpreting the data.

There are three sets of time-dependent data produced by each experiment:

(1) A photovoltaic representation of the flash

(2) A pressure profile of the gas

(3) The optical transmittance of the aerosol

These data are used to produce the following functions:

(1) $W_f(t)$, time-dependent flash power

(2) $T_g(t)$, time-dependent gas temperature

(3) $\gamma(t)$, time-dependent energy absorptivity of the gas

The first step in obtaining these functions is to digitize the photovoltaic profile of the flash power and the pressure profile. This was done by using a

Moseley Model F-3B Line Follower in conjunction with a Honeywell S3084 Data Logging System and a Teletype Model 33 printer and paper tape punch unit for recording the digitized data. The paper tape was then read onto magnetic tape and converted into meaningful data for the Univac 1108 computer.

All independent experimental and instrument parameters were recorded on computer code sheets, transcribed onto IBM cards, and merged with the digitized data on a single magnetic tape.

TIME-DEPENDENT FLASH POWER

The photodiode output is proportional to the intensity of the flash. Therefore, the photodiode scope trace is the time-dependent rate at which energy is available to the aerosol multiplied by an appropriate constant, k, as

$$W_f(t) = kw(t) \tag{B1}$$

where,

$W_f(t)$ = Flash power (watts)

w (t) = Diode output (volts).

Integrating Equation B1 yields

$$\int W_f(t)dt = E_c = k\int w(t)\,dt, \tag{B2}$$

where E_c is the calorimeter measurement in joules.

Therefore, k is defined as

$$k \equiv E_c / \int w(t)dt. \tag{B3}$$

Substitution into Equation B1 yields

$$W_f(t) = E_c \frac{w(t)}{\int w(t)dt} . \tag{B4}$$

This is the equation used in the computer program to calculate time-dependent flash power. E_c is fed into the computer as an independent parameter and w(t) is available as a digitized scope trace.

GAS TEMPERATURE AND ENTHALPY

Gas temperature is calculated from the digitized pressure trace P(t), initial pressure P_o, and necessary scale factors as

$$T_g(t) = f(P_o, P(t)). \tag{B5}$$

The equation-of-state for an ideal gas is used in calculating helium temperatures as

$$T_g(t)_{He} = 300^\circ K \, P(t)/P_o. \tag{B6}$$

For hydrogen at the range of test pressures covered in these experiments, the ideal gas law is invalid above 2000°K because of the dissociation of the H_2 molecule. The equation-of-state for one mole of a dissociating gas can be written as

$$\frac{PV}{RT_g} = Z(P, T_g), \qquad \text{(From NACA TN 3270, 1955)} \tag{B7}$$

where $Z(P, T_g)$ is the compressibility factor, given by

$$Z(P, T_g) = 1 + x, \qquad \text{(From NACA TN 3270, 1955)} \qquad \text{(B8)}$$

and x is the degree of dissociation (0→1), given by

$$x = \sqrt{K/(K + 4P)}\,, \qquad \text{(B9)}$$

where K is the equilibrium constant determined for the reaction $H_2 \rightleftarrows 2H$. For hydrogen

$$\text{Log}_{10}K = 6.20 - 2.354(10^4/T_g) \text{ (From NASA SP 3005, 1963).} \qquad \text{(B10)}$$

Equation B7 then becomes

$$\frac{PV}{RT_g} = 1 + \sqrt{K/(K + 4P)} \qquad \text{(B11)}$$

for n_o initial moles

$$\frac{PV}{RT_g} = \left\{1 + \sqrt{K/(K + 4P)}\right\} n_o, \qquad \text{(B12)}$$

where

$$n_o = \frac{P_o V}{RT_o}\,. \qquad \text{(B13)}$$

Rearrangement yields

$$\frac{P\ T_o}{P_o\ T_g} = 1 + \sqrt{K/(K + 4P)}\,. \qquad \text{(B14)}$$

Defining

$$y \equiv 10^4/T_g, \qquad \text{(B15)}$$

produces

$$10^{-4}\frac{PT_o}{P_o}\ y = 1 + \sqrt{K(y)/(K(y) + 4P)} \tag{B16}$$

$$F(y) = G(y).$$

A value of y (and hence T_g) can be found by iterating the functions of Equation B16. The computer program calculates the gas temperature of hydrogen in this manner.

Once the temperature of the gas has been determined, the change in specific enthalpy, Δh, for helium can be calculated from

$$\Delta h = \int_{300}^{Tg} C_p\ Tg = C_p(Tg - 300), \tag{B17}$$

where C_p is the specific heat capacity at constant pressure.

However, with hydrogen, the latent heat of dissociation, ℓ_D, and the degree of dissociation, x, must be considered. Thus, for hydrogen

$$\Delta h = (1 - x)\Delta h_{H_2} + 2x\Delta h_H + x\ell_D \tag{B18}$$

$$\Delta h_{H_2} = \int_{300}^{Tg} Cp_{H_2}(T)dTg \tag{B19}$$

$$\Delta h_H = \int_{300}^{Tg} Cp_H dTg = Cp_H(Tg - 300)\ . \tag{B20}$$

For Equation B19, Cp_{H_2} appears in the computer as an algebraic equation. Once the change in specific enthalpy has been calculated, the total change is found (for both gasses) by multiplying Δh by the initial number of moles of gas, n_o, as

$$\Delta H(T_g) = n_o\Delta h(T_g)\ , \tag{B21}$$

where

$$n_o = (V/V_{STP})(P_o/P_{STP})(300/T_{STP})$$

V = volume of test cell (cm^3)

V_{STP} = 22 400 cm^3

P_o = initial pressure (atm)

P_{STP} = 1 atm

T_{STP} = 273°K

Gas temperature and change in enthalpy for both hydrogen and helium is calculated and stored as part of the data reduction program.

ABSORPTIVITY

Time-resolved absorptivity, γ, is defined as

$$\gamma(t) = W_g(t)/W_f(t) , \qquad \text{(B22)}$$

where $W_g(t)$ is the rate at which energy is entering the gas and $W_f(t)$ is the rate at which flash energy is available to the aerosol. The latter, $W_f(t)$, has been calculated as outlined in the Time-Dependent Flash Power section of this appendix. The former, $W_g(t)$, is calculated by differentiating Equation B21 with respect to time as

$$W_g(t) = d(\Delta H)/dt . \qquad \text{(B23)}$$

From a computational standpoint, the process is simple because $\Delta H(t)$ and $W_f(t)$ had already been calculated; thus, the time-resolved absorptivity is part of the computer reduction routines.

Page intentionally left blank

Appendix C

COMPUTING PROGRAMS

This appendix describes the numerical techniques used to solve the flash-heating temperature history.

ANALYTIC MODEL

Differential Equations 29 and 30 have undergone several program modifications to appraise the contribution of its component factors. The final form of these equations is:

$$\Delta T_i \equiv dT_i = \frac{3}{a_i \delta c} \left\{ \varepsilon A_\omega Q_\omega \alpha_\omega \alpha_g / A + \varepsilon (\Sigma_j 4\pi a_j^2 \varepsilon\sigma T_j^4)(1-G)\ \alpha_g / A \right.$$

$$\left. - \varepsilon\sigma T_i^4 \alpha_g - \frac{K}{a_i}(T_i - T_g) \right\} . \Delta t, \quad (i = 1, 2, \ldots, N) \tag{C1}$$

and

$$\Delta t_g \equiv dt_g = \frac{1}{V_g \delta_g C_g} \left\{ \Sigma_j 4\pi a_j^2 \frac{K}{a_j} (T_i - T_g) - HA_\omega (T_g - T_\omega) \right\} . \Delta t . \tag{C2}$$

The transmittance terms α_ω and α_g are arbitrary time-dependent functions. For the case where no seed evaporation occurs, these are:

$$\alpha_{\omega} = F \text{ (geometric view factor)} \tag{C3}$$

and,

$$\alpha_{g} = 1.0 . \tag{C4}$$

In the case with evaporation of seed and subsequent wall deposition these were given values of

$$\alpha_{\omega} = 1.0 - \frac{0.6}{\pi}\left[\frac{\pi}{2} - \tan^{-1}(1.1 - 500t)\right] \tag{C5}$$

and,

$$\alpha_{g} = 0.1 + (F - 0.1)\left[\frac{\pi}{2} - \tan^{-1}(1200t - 2.4)\right]/\pi . \tag{C6}$$

Equation C1 and C2 can be generalized as functions of seed temperatures and gas temperature and written as

$$\Delta T_i = F(T_i, T_g).\Delta t \equiv F(T, T_g) \tag{C7}$$

and,

$$\Delta t_g = G(T_i, T_g).\Delta t = G(T, T_g), \quad (i = 1, 2, \ldots, N) . \tag{C8}$$

The numerical technique chosen to compute the temperature at t+ Δt, given T_o and T_{go} at time t, was a mixture of Euler's method and Euler's modified method (ref. 18). The value of seed temperature was given a first estimate of

$$T_1^{\,1} = T_o + F(T_o, T_{go}), \tag{C9}$$

where the superscript is the estimation order. Then subsequent estimates were given by

$$T_1^{\,j+1} = T_o + \left\{F(T_o, T_{go}) + F(T_1^{\,j}, T_{go})\right\}/2.0 . \tag{C10}$$

It was found that an estimation order of 2 gave good agreement with other numerical techniques. This gives a modified Euler's approximation for the seed temperature. Gas temperatures were given by a simpler single-step Euler's method as

$$T_{g1} = T_{go} + G(T_1^{j+1}, T_{go}) .$$

Equations C1 and C2 were also programmed using a Runge-Kutta method and Milne's method. All three methods gave good agreement with cases checked. The described method was chosen to run the case because of shorter computing time.

RAW DATA

Figure C1 is a representation of the steps involved in reducing and storing raw data. All programs for the Univac 1108 are written in Fortran. The hydrogen and helium data were processed separately. Six tapes contain the digitized data, three for each gas. These tapes, with the program operation instructions and data formats, will be stored for two years by the Donald W. Douglas Laboratories for any future reference.

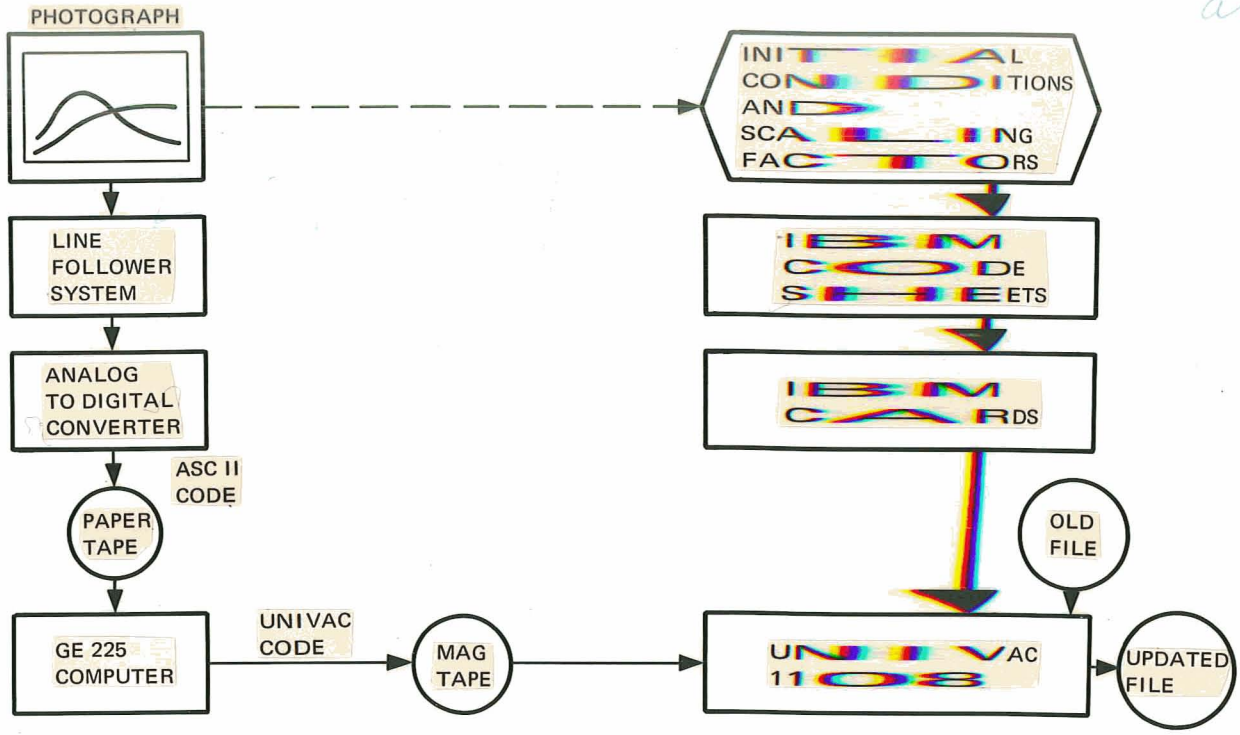

Figure C-1. Automatic Process Used in Reduction and Storage of Raw Data

REFERENCES

1. Lanzo, C. D. ; and Ragsdale, R. G. : Heat Transfer to a Seeded Flowing Gas from an Arc Enclosed by a Quartz Tube. Proceedings of the Heat Transfer and Fluid Mechanics Institute, 1964.

2. Krascella, N. L. : Tables of the Composition, Opacity, and Thermodynamic Properties of Hydrogen at High Temperatures. NASA SP-3005, 1963.

3. Lanzo, C. D. ; and Ragsdale, R. G. : NASA TND-1405, September 1962.

4. Masser, C. C. : NASA TND 3197, January 1965.

5. McAlister, J. A. ; Keng, E. Y. H. ; and Orr, C. Jr. : Heat Transfer to a Gas Containing a Cloud of Particles. NASA Project A-635-002, NsG-273-62, June 1965.

6. Burkig, V. W. : Thermal Absorption in Seeded Gases. Contract NASw-1310, McDonnell Douglas Report DAC-59985, January 1967.

7. Knapp, D. E. ; Burkig, V. C. ; and Cory, J. S. : Flash Heating of Seeded Gases. Presented at AIAA 3rd propulsion Conference, 1967, AIAA paper 67-501.

8. Masataka, O. ; and Zung, J. T. : Evaporation Condensation Coefficient for Small Droplets. J. Chan Physics Vol. 46 No. 5, 1962, pp. 1580-1585.

9. Monchick, L; and Reiss, H.: Studies of Evaporation of Small Droplets. JCP Vol. 22 No. 5, 1954, pp. 831-836.

10. Dushman, S.; and Lafferty, J. M.: Scientific Foundations of Vacuum Techniques. Wiley 2nd ed., 1962, Chapter 6.

11. Born and Wolf. Principals of Optics. 3rd ed. Pergamon (1965), pp. 659-573.

12. Cadle, R. D.: Particle Size. Reinhold, 1965, pp. 52-65.

13. Sparrow, E. M.: Radiation Heat Transfer. Brooks, 1966.

14. Soo, S. L.: Gas-Solid Suspensions at High Temperatures. JAP Vol. 34 No. 6 (63), pp. 1689-1696.

15. Spitzer, Lyman: Physics of Fully Ionized Gases. Interscience 2nd ed., 1965, pp. 148.

16. Visvanathan, S.: Free Carrier Absorption Arising from Impurities in Semiconductors. Physical Rev. Vol. 120 No. 2, 1960, pp. 379-380.

17. Sleicker, C. A.; and Churchill, S. W.: Radiant Heating of Dispersed Particles. Indus. & Engr. Chem. Volume 48 No. 10, 1956, pp. 1819-1824.

18. Scarbough, J. B.: Numerical Mathemtaical Analysis. Fourth ed., The John Hopkins Press, Baltimore, 1958, pp. 248-254.